Atmos. Meas. Tech. Discuss., 4, 7337–7403, 2011
www.atmos-meas-tech-discuss.net/4/7337/2011/
doi:10.5194/amtd-4-7337-2011

Atmospheric Measurement Techniques Discussions

Correction technique for raman water vapor lidar signal dependent bias and suitability for water vapor trend monitoring in the upper troposphere

D. N. Whiteman[1], M. Cadirola[2], D. Venable[3], M. Calhoun[3], L. Miloshevich[4], K. Vermeesch[5], L. Twigg[5], A. Dirisu[6], D. Hurst[7], E. Hall[7], A. Jordan[7], and H. Vömel[8]

[1]NASA/GSFC, Greenbelt, MD 20771, USA
[2]Ecotronics, LLC, Clarksburg, MD 20871, USA
[3]Howard University, Washington, DC, USA
[4]Milo Scientific, LLC, Lafayette, CO 80026, USA
[5]SSAI, Lanham, MD, USA
[6]Oak Ridge Associated Universities, Oak Ridge, 37381, TN, USA

[7]Cooperative Institute for Research in Environmental Sciences, University of Colorado, Boulder, Colorado 80309 and NOAA Earth System Research Laboratory, Global Monitoring Division, Boulder, Colorado 80305, USA
[8]Lindenberg Observatory, Lindenberg, Germany
Received: 30 June 2011 – Accepted: 1 August 2011 – Published: 12 December 2011

Correspondence to: D. N. Whiteman (david.n.whiteman@nasa.gov)

Published by Copernicus Publications on behalf of the European Geosciences Union.

Abstract

The MOHAVE-2009 campaign brought together diverse instrumentation for measuring atmospheric water vapor. We report on the participation of the ALVICE mobile laboratory in the MOHAVE-2009 campaign. In an appendix we also report on the performance of the corrected Vaisala RS92 radiosonde during the campaign. A new radiosonde based calibration algorithm is presented that reduces the influence of atmospheric variability on the derived calibration constant. The MOHAVE-2009 campaign permitted all Raman lidar systems participating to discover and address measurement biases in the upper troposphere and lower stratosphere. The ALVICE lidar system was found to possess a wet bias which was attributed to fluorescence of insect material that was deposited on the telescope early in the mission. A correction technique is derived and applied to the ALVICE lidar water vapor profiles. Other sources of wet biases are discussed and data from other Raman lidar systems are investigated revealing that wet biases in upper tropospheric and lower stratospheric water vapor measurements appear to be quite common in Raman lidar systems. Lower stratospheric climatology of water vapor is investigated both as a means to check for the existence of these wet biases in Raman lidar data and as a source of correction for the data. The correction is offered as a general method to both quality control Raman water vapor lidar data and to correct those data that have signal-dependent bias. The influence of the correction is shown to be small at regions in the upper troposphere where recent work indicates detection of trends in atmospheric water vapor may be most resistant to additional noise sources. The correction shown here holds promise for permitting useful upper tropospheric water vapor profiles to be consistently measured by Raman lidar within NDACC and elsewhere despite the prevalence of instrumental and atmospheric effects that can contaminate the very low signal to noise measurements in the UT.

AMTD
4, 7337–7403, 2011

1 Introduction

Water vapor is an important atmospheric constituent that affects weather, climate and atmospheric chemistry. Climate model predictions indicate that water vapor will increase in the atmosphere as temperatures increase due to climate change (Held and Soden, 2006; Boers and Meijgaard, 2009; Whiteman et al., 2011b). The largest changes are expected in the upper troposphere where model predictions show annual increases of up to 1 % or more during the current century (Soden et al., 2005; Boers and Meijgaard, 2009; Whiteman et al., 2011b). International networks such as the Raman water vapor lidar network within the Network for the Detection of Atmospheric Composition Change (NDACC) and the Global Climate Observing System Reference Upper Air Network (GRUAN) are being established in response to the need to monitor water vapor trends in the atmosphere.

MOHAVE-2009 (Leblanc et al., 2011b) was held in October 2009 at Table Mountain, CA with the goal of characterizing a large suite of water vapor instrumentation used within NDACC. Information about the campaign can be found at http://tmf-lidar.jpl.nasa.gov/campaigns/mohave2009.htm. Here we report on measurements made by the mobile system referred to as ALVICE (Atmospheric Laboratory for Validation, Interagency Collaboration and Education) and the performance of the corrected Vaisala RS92 radiosonde during MOHAVE-2009. A new radiosonde calibration technique that reduces the influence of atmospheric variability on the derived lidar calibration constant is developed and tested. We use the lidar measurements to motivate a discussion of lidar correction techniques with application to trend detection. We discuss wet biases in Raman water vapor measurements in general and specifically a wet bias present in the ALVICE lidar data due to what we believe to be fluorescence of insect material that was deposited on the telescope early in the MOHAVE-2009 mission. A correction is developed to address this wet bias and applied to the ALVICE Raman lidar data processed for MOHAVE-2009. We discuss the implications of wet biases in Raman lidar measurements on trend detection and propose the use of lower stratospheric water

AMTD
4, 7337–7403, 2011

vapor climatology for quality control and correction of Raman water vapor lidar measurements intended for scientific studies in the troposphere.

2 ALVICE

The instrumentation comprising ALVICE is contained in a mobile environmentally-controlled trailer for deploying to field locations. The system contains a large suite of instrumentation for quantifying atmospheric water vapor, aerosols, clouds and temperature. The instrumentation now housed within the trailer includes an upgraded version of the Raman Airborne Spectroscopic Lidar (RASL) (Whiteman et al., 2007) mounted in an upward looking configuration for performing vertical profiling (Whiteman et al., 2010). The additional instrumentation includes a ventilated chamber, referred to as THPref (Temperature-Humidity-Pressure Reference), for continuous surface reference data and for characterizing radiosonde accuracy prior to launch, a SuomiNet (Ware et al., 2000) GPS instrument for total column water measurements, stabilized calibration lamp for asessing lidar channel optical throughout, and equipment for launching Vaisala RS92 radiosondes and Cryogenic Frostpoint Hygrometers (CFH).

2.1 ALVICE Lidar

The Raman Airborne Spectroscopic Lidar (RASL) mounted in an upward-looking configuration forms the heart of the lidar system contained within ALVICE and has been described previously in the literature (Whiteman et al., 2007, 2010). Since the time of those publications and prior to the MOHAVE-2009 campaign the only significant lidar system modifications were the addition of rotational Raman temperature measurement capability and the use of a thermo-electrically cooled PMT for the water vapor channel measurements. Therefore, just a brief summary of the lidar instrumentation will be given here.

AMTD
4, 7337–7403, 2011

The Raman lidar contained in the ALVICE trailer uses an injection-seeded Continuum 9050 Nd:YAG laser operating at the frequency-tripled wavelength of 354.7 nm and emits pulses with approximately 300–350 mj of energy at a rate of 50 Hz. The backscattered signals from the atmosphere are gathered by a 0.6 m telescope and separated into 10 optical channels using both dichroic beamsplitters (for the main Raman and aerosol parameters) and a fiber optic (for the rotational Raman temperature channels). Both analog-to-digital and photon counting data acquisition are used and the minimum range resolution of the system is 7.5 m. To maximize the signal-to-noise of the water vapor measurement in the dry UTLS region, in addition to the cooled water vapor PMT, narrow telescope field-of-view (250 μradians) and water vapor interference filter (0.25 nm) are used.

During MOHAVE-2009, profiles were acquired every 2 min to capture the evolution of the highly variable water vapor environment at Table Mountain. Optical channels in use during MOHAVE-2009 included Raman water vapor, nitrogen, liquid/ice water, 3 different unpolarized aerosol channels, parallel and perpendicular polarization aerosol channels and two rotational Raman channels similar to that described in DiGirolamo et al. (2004) except that in this new configuration a filter polychromator approach (Behrendt and Reichardt, 2000) is used and the Stokes part of the spectrum is sampled as opposed to the anti-Stokes as in DiGirolamo et al. (2004). The quicklook ALVICE temperature data have been compared with the Michelson Interferometer for Passive Atmospheric Sounding (MIPAS) made during MOHAVE-2009 (Stiller et al., 2011) and indicated that MIPAS temperatures are 1–2 K higher than lidar temperatures below the tropopause and lower than lidar temperatures above the tropopause. This same relationship was found in other comparisons (Stiller et al., 2011).

The Raman lidar contained in ALVICE operated on 13 nights during MOHAVE-2009 acquiring approximately 88 h of measurements of water vapor, aerosols, clouds and temperature over the period of 12–27 October 2009.

AMTD
4, 7337–7403, 2011

2.2 ALVICE ancillary instrumentation and measurements

MOHAVE-2009 presented the first opportunity to deploy all of the ALVICE instrumentation during a field campaign. All balloon preparations and launches for both Vaisala RS92 and Cryogenic Frostpoint Hygrometer (CFH) (Vömel et al., 2007a) were led by Table Mountain Facility (TMF) staff but several balloons included dual RS92 launches where the second RS92 was prepared by Goddard Space Flight Center (GSFC) staff and the data were received and recorded using the ALVICE ground station. These simultaneous RS92 flights permitted the study of radiosonde data consistency and production variability. There were also several launches of the NOAA frostpoint hygrometer (Hurst et al., 2011b). The frostpoint hygrometer measures the frostpoint temperature of the air based on the chilled-mirror principle (Mastenbrook and Dinger, 1961), and uses a cryogenic heat sink for fast response and accurate measurement under very dry conditions (Vömel et al., 2007a; Hurst et al., 2011b). The frostpoint measurements are converted to RH and mixing ratio using temperature (T) and pressure (P) measured by the RS92, respectively, with an estimated total uncertainty of ±4 % at the surface increasing to ±10 % in the lower stratosphere. An extensive discussion of the radiosonde and frostpoint measurements during MOHAVE-2009 is contained in Hurst et al. (2011b). Henceforth, the CFH and NOAA frostpoints will be considered equivalently, as done in Hurst et al. (2011b), and referred to as FP.

THPref

The ALVICE mobile trailer includes a surface reference system referred to as THPref (Temperature-Humidity-Pressure Reference) that provides NIST traceable measurements of temperature, relative humidity and pressure and contains a ventilated chamber for characterizing radiosonde accuracy prior to launch. The time series of surface data and derived products is shown in Fig. 1 where the SuomiNet total column water data are reported here as well for convenience. The measurements acquired during the time that radiosondes were inserted into the ventilated chamber are shown by red dots in Fig. 1 and were used to study radiosonde calibration errors and corrections as

AMTD
4, 7337–7403, 2011

described in Appendix A. The results discussed there indicate that the estimated total RH uncertainty for corrected RS92 measurements during the MOHAVE-2009 campaign were ±(5 % + 0.5 % RH) for RH > 10 % and ±(7 % + 0.5 % RH) for RH ≤ 10 %, which corresponds to an uncertainty of ±6 % at 50 % RH, ±10 % at 10 % RH, and ±24 % at 3 % RH. These error assessments for the corrected data are altitude independent. By contrast, the error characteristics of uncorrected RS92 data have a significant altitude dependence (Miloshevich et al., 2009).

3 Previous measurements and contamination during MOHAVE-2009

Prior to MOHAVE-2009, the ALVICE system was deployed to the Howard University Beltsville Campus in Beltsville, MD for the WAVES_2009 campaign in January–April, 2009. During that campaign, long duration nighttime measurements of water vapor mixing ratio were made using the ALVICE lidar system. Four frostpoint hygrometers were launched during this campaign. Good agreement was found between ALVICE lidar, frostpoint hygrometer and available MLS data in the lower stratosphere. There was no indication of a moist bias in the ALICE lidar UTLS water vapor measurements during WAVES_2009 and therefore we believe that the ALVICE lidar arrived for MOHAVE-2009 free of any significant fluorescence. The measurements during WAVES_2009 were made with the telescope protected from the outside environment through the use of an optical window. This window was removed at the beginning of MOHAVE-2009 to reproduce the measurement configuration of the ALVICE system during MOHAVE-II in 2007 (Whiteman et al., 2010) where the window was not used so as to maximize the signal returns.

The weather at Table Mountain during MOHAVE-2009, however, presented some quite different conditions than encountered during MOHAVE-II. There were periods of warm weather during which significant populations of flying insects were present in the vicinity of the lidar systems. On the night of 16 October, a large number of insects was attracted to the UV laser beam, which is emitted along the optical axis of the telescope. Insects that were attracted to the UV laser radiation were able to follow the laser beam

AMTD
4, 7337–7403, 2011

into the trailer and enter both the telescope and the laser. Signals were completely lost during this data acquisition session due to insects obscuring the field stop of the telescope thus operations were curtailed early on this night. Considerable effort was expended in cleaning the laser and the telescope and in re-installing the protective window that had been used in WAVES_2009 over the telescope. A proper cleaning of the ALVICE telescope receiver, however, requires an effort that was deemed too complicated and time consuming to attempt during a field campaign. Therefore, a noticeable amount of insect residue remained on the telescope primary and other components of the receiving optics after this cleaning. This was the configuration of the lidar receiver optical system for the measurements analyzed here. As will be described below, excess signal was found in the water vapor channel in the UTLS portion of the profile. Some insects are known to have strong fluorescence signature when stimulated with UV radiation (Byrdegaard et al., 2009). Therefore, it is believed that this additional signal was due to the fluorescence of the insect residue that remained deposited on the lidar telescope.

In the analysis that follows, the additional signal in the water vapor channel due to fluorescence is considered to be constant during the MOHAVE campaign for the following reasons. After the insect incident on 16 October, a window was installed over the ALVICE telescope. This window prevented further contamination inside the ALVICE trailer. Also, a large industrial fan (0.9 m diameter, 340 000 l min^{-1}) was mounted on top of the trailer and blew across the window during lidar operation periods to prevent any significant material buildup on the window. In addition, the window was washed prior to every subsequent operation period during MOHAVE. Finally, as we will point out later in Sect. 7.0, the analysis of the data does not indicate significant variation of the correction value during the MOHAVE campaign.

4 The challenge of UTLS water vapor measurements using Raman lidar

The literature and other analyses reveal that there are three general causes of wet biases in Raman lidar UT water vapor measurements. The apparent excess amount

AMTD
4, 7337–7403, 2011

of water vapor can be due to (1) the lidar instrument itself, (2) the data processing or (3) atmospheric contaminants. The MOHAVE history reveals that all three of these have played a role in the evolution of instrumental development and data processing described in Sect. 8.

4.1 Biases due to instrumental effects

There are earlier studies of upper tropospheric and lower stratospheric water vapor measurements using Raman lidar that have shown a wet bias. Sherlock et al. (1999) noted excess water vapor signal corresponding to a wet bias of approximately 80 ppmv due to fluorescence of their fiber optic. Replacement of this fiber by an OH-rich fiber reduced the fluorescence contamination to 8 ppmv or less. However the authors state that "...although here absorption of the elastic-backscatter signal occurs in the fiber-optic cable used for signal transfer, it could arise in any optical component. Thus fluorescence processes are a potential source of systematic error in Raman Stokes measurements, particularly in the case of water vapor, where the signals are weak and susceptible to contamination."

4.2 Biases due to data processing

Ferrare et al. (2004) discuss the Atmospheric Radiation Measurement (ARM)–First International Satellite Cloud Climatology Project (ISCCP) Regional Experiment (FIRE) Water Vapor Experiment (AFWEX) field campaign that took place in December 2000 at the Southern Great Plains site of the Department of Energy. The initial results showed the CART Raman lidar to possess a wet bias in the upper troposphere with respect to the reference airborne water vapor instrumentation. The CART Raman lidar is calibrated based on a total column water comparison with the ARM microwave radiometer so the wet bias was found to be due to an error in the overlap correction used in the lidar data processing (Ferrare et al., 2004) that influenced the magnitude of the total column water calculated from lidar.

AMTD
4, 7337–7403, 2011

Whiteman et al. (2006c) report on the results of the AWEX-G (AIRS Water Vapor Experiment-Ground) field campaign held at the same SGP site in 2003. This campaign was staged due to the early results of the NASA Aqua satellite validation program that indicated significant disagreement between Raman lidar and Vaisala radiosonde measurements of water vapor. Water vapor profiles from both Raman lidar and Vaisala RS90 were being used as sources of calibration/validation data in AIRS fast forward model studies. The simulated radiances calculated using the lidar and radiosonde profiles in the AIRS forward model implied a disagreement of approximately 25 % in the upper tropospheric water vapor measurements between the Scanning Raman Lidar and the Vaisala radiosondes. A Raman lidar UT wet bias of approximately 12 % was found. A dry bias in the radiosondes was also quantified (Miloshevich et al., 2006). The lidar wet bias was corrected by accounting for the temperature dependence of Raman scattering and improving the lidar overlap function (Whiteman et al., 2006c). The Vaisala dry bias was addressed by empirical correction (Miloshevich et al., 2006) of the RS90 to obtain best agreement with frostpoint hygrometer. After applying these independently determined corrections, the Scanning Raman lidar measurements and those of empirically corrected Vaisala radiosonde were found to agree at the 5 % level in the upper troposphere.

4.3 Biases due to atmospheric constituents

In addition to the fluorescence of atmospheric insect remains that led to the moist bias in the ALVICE Raman lidar data reported here, there is other evidence in the literature of direct fluorescence of atmospheric particles presenting a contaminating signal to Raman water vapor lidars. Immler et al. (2005) detected enhancements in their water vapor signal due to the fluorescence of lower stratospheric aerosols. Furthermore, aerosols of biological origin such as bacteria, spores or pollen and leaf matter are found in the atmosphere and can present a strong fluorescence signature that, due to the spectral nature of the fluorescence, can create an apparent wet bias in the water vapor measurement (Saito et al., 2010). The fluorescence signature of individual aerosol

AMTD
4, 7337–7403, 2011

particles in the ambient atmosphere has been studied showing that a small percentage of these particles possesses a strong fluorescence signature (Pan et al., 1999; Pinnick et al., 2004) in the spectral region where Raman water vapor lidar measurements are made. These results confirm earlier work (Gelbwachs and Birnbaum, 1973) indicating that aerosol fluorescence posed potential problems for Raman lidar measurements of trace gases.

4.4 Wet biases in other lidar systems

Wet biases in UTLS Raman water vapor lidar data are not limited to just the Raman lidar systems that participated in the MOHAVE campaigns. Study of the data from other well-known Raman lidar systems indicate the presence of wet UT biases as well. For example, 5 yr of CART Raman lidar (Turner et al., 2002; Ferrare et al., 2004) data have been studied covering the period of 1998–2003. A persistent wet bias of approximately 8–12 ppmv was found in the lower stratosphere. Approximately 10 yr of data from the Tor-Vergata lidar outside of Rome (Dionisi et al., 2009) have been studied with the conclusion that a persistent wet bias of approximately 10 ppmv in the lower stratosphere exists as well (Gian Luigi Liberti, personal communication, June, 2011). Selected data from ten years of measurements with the Meteorological Research Institute Raman lidar in Tsukuba, Japan (Sakai et al., 2007) have also been studied revealing a persistent wet LS bias of approximately 50 ppmv (Tetsu Sakai, personal communication, May, 2011).

Furthermore, it should be noted that the wet bias present in the CART Raman lidar data record between 1998–2003 encompasses the period of the AFWEX experiment (Ferrare et al., 2004), during which the finally processed CART Raman lidar data agreed well with the reference in the UT. It may be that the focus of the UT investigations during the AFWEX mission, which was on the integrated water between 7 and 12 km, masked the presence of this small moist bias that manifested itself primarily at altitudes above 12 km. Fortunately, the complete raw data from the lidar are archived within the DOE/ARM program permitting this question to be studied further.

AMTD
4, 7337–7403, 2011

The details above indicate that wet UTLS biases in Raman lidar data are rather common and derive from various sources including atmospheric, instrumental and algorithmic effects. The apparent frequent occurrence of these wet biases can be related to the very large challenge of measuring the low values of water vapor mixing ratio in the UTLS using the Raman lidar technique. Recent ALVICE Raman lidar measurements acquired in the Greenbelt, MD vicinity indicate that the signal to noise ratio of the water vapor measurements at an altitude of 13 km m.s.l. is approximately the same as the signal to noise ratio of the measurements of Raman nitrogen at 60 km or the Rayleigh signal at 80 km. In other words, because of the small water vapor amounts in the UTLS very low signal to noise ratios exist and the potential for small error sources to bias the data is thus more magnified.

The main point to be made concerning the preceeding discussion is that the potential of a bias being present or developing in a Raman lidar measurement of UTLS water vapor seems too high to not be concerned with it on a routine basis. Correcting systematic effects such as this is consistent with the recommendations of the Joint Committee on Guides in Metrology in their Guide to the Expression of Uncertainty in Measurements (GUM) (JCGM/GUM, 2008) where it is stated that "Systematic error, like random error, cannot be eliminated but it too can often be reduced. If a systematic error arises from a recognized effect of an influence quantity on a measurement result, hereafter termed a systematic effect, the effect can be quantified and, if it is significant in size relative to the required accuracy of the measurement, a correction ... or correction factor ... can be applied to compensate for the effect. It is assumed that, after correction, the expectation or expected value of the error arising from a systematic effect is zero." and "It is assumed that the result of a measurement has been corrected for all recognized significant systematic effects and that every effort has been made to identify such effects." Following these recommendations, we next present a method for assessing the presence of and correcting for signal-dependent biases in UTLS Raman water vapor lidar data.

AMTD
4, 7337–7403, 2011

5 Mathematical model for signal dependent water vapor bias

The following model is developed to address the situation where additional signal is present in the water vapor channel of a Raman lidar and that additional signal is proportional to the magnitude of the signal backscattered at the laser wavelength. This situation could be created by fluorescence of optical materials in the lidar receiver or insufficient blockage of any of the Rayleigh-Mie, Raman N_2 or O_2 signals in the Raman water vapor channel. The case of excess signal in the water vapor channel due to insufficient blocking of the Rayleigh-Mie signal or fluorescence will be handled here. The case for leakage of the Raman nitrogen or oxygen return is discussed in Sect. 5.1. Note that a situation of excess signal due to fluorescence of airborne particles as described in Immler et al. (2005) would not be addressed by this correction technique.

We will use the formulation of the lidar equations found in Whiteman et al. (2003a); Whiteman (2003b). The water vapor mass mixing ratio may be expressed as

$$w = k\frac{O_N(r)}{O_H(r)}\frac{F_N(T)}{F_H(T)}\frac{P(\lambda_H,r)}{P(\lambda_N,r)}\frac{\frac{d\sigma_N(\pi)}{d\Omega}}{\frac{d\sigma_H(\pi)}{d\Omega}}\frac{\xi(\lambda_N)}{\xi(\lambda_H)}\Delta\tau(\lambda_N,\lambda_H,r) \quad (1)$$

where the constant of proportionality, k, has a value of approximately 0.486 and is determined by the molecular weights of water vapor and nitrogen and the fractional abundance of nitrogen in the atmosphere (Whiteman, 2003b). $P(\lambda_X,r)$ is the backscattered power (after subtracting any background contribution due, for example, to skylight or detector noise) received at λ_X due to Raman scattering from either water vapor (H) or nitrogen (N) as a function of range, r. $O_X(r)$ is the overlap function for either Raman channel. $\xi(\lambda_X)$ is the total lidar receiver optical efficiency at the wavelengths of the water vapor or nitrogen signals and includes factors such as the reflectivity of the telescope, the transmission of conditioning optics, the transmission of any filters and the quantum efficiency of the detector. $\frac{d\sigma_X(\pi)}{d\Omega}$ is shorthand notation for the Raman backscatter cross section when stimulated at the laser wavelength. $F_X(T)$ is a factor that carries all the temperature dependence of the Raman scattering process and thus

AMTD
4, 7337–7403, 2011

appears as a multiplier of the traditional Raman lidar equation (Whiteman et al., 2003a). $\Delta\tau(\lambda_N,\lambda_H,r)$ is the "differential transmission" between the λ_H and λ_N and is calculated typically from a radiosonde measurement of atmospheric density.

Consider now the situation where there is excess signal in the water vapor channel due to a signal-dependent source such as interference filter bleedthrough or fluorescence. This dependence is expressed as $\zeta_0 P(\lambda_R,r)$ in the following equations, where ζ_0 is the ratio of the additional, spurious signal in the water vapor channel and the Rayleigh-Mie signal at the laser wavelength, which is represented by $P(\lambda_R,r)$. We will assume that the magnitude of any such signal dependent bias in the nitrogen channel is negligible in the ratio shown in Eq. (1). This assumption is based on the typical situation where the Raman nitrogen signal strength is at least 6 orders of magnitude larger than that from water vapor in the upper troposphere below which the signal dependent biases considered here become increasingly less significant due to the typically much larger water vapor mixing ratios at lower altitudes.

If the water vapor channel is contaminated by an amount proportional to the backscattered Rayleigh-Mie signal intensity, the apparent water vapor mixing ratio, w^* can be expressed

$$w^* = k\frac{O_N(r)}{O_H(r)}\frac{F_N(T)}{F_H(T)}\frac{P(\lambda_H,r)+\zeta_0 P(\lambda_R,r)}{P(\lambda_N,r)}\frac{\frac{d\sigma_N(\pi)}{d\Omega}}{\frac{d\sigma_H(\pi)}{d\Omega}}\frac{\xi(\lambda_N)}{\xi(\lambda_H)} \times\Delta\tau(\lambda_N,\lambda_H,r) \quad (2)$$

$$= k\frac{O_N(r)}{O_H(r)}\frac{F_N(T)}{F_H(T)}\frac{P(\lambda_H,r)}{P(\lambda_N,r)}\frac{\frac{d\sigma_N(\pi)}{d\Omega}}{\frac{d\sigma_H(\pi)}{d\Omega}}\frac{\xi(\lambda_N)}{\xi(\lambda_H)} \times\Delta\tau(\lambda_N,\lambda_H,r)\left(1+\frac{\zeta_0 P(\lambda_R,r)}{P(\lambda_H,r)}\right) \quad (3)$$

$$= w\left(1+\frac{\zeta_0 P(\lambda_R,r)}{P(\lambda_H,r)}\right) \quad (4)$$

AMTD
4, 7337–7403, 2011

or the actual mixing ratio, w, is given by

$$w = w^* \frac{P(\lambda_H, r)}{P(\lambda_H, r) + \zeta_0 P(\lambda_R, r)} \quad (5)$$

where the value of ζ_0 can be determined by comparison of the lidar mixing ratio profile with a reference profile. Equation (5) gives an exact solution when the value of ζ_0 is known. Under certain assumptions the correction for the excess signal can be approximated by a simple subtraction in mixing ratio space as will now be shown.

Working with Eq. (4) and assuming that no significant aerosol scattering is present where the contamination is significant, generally in the upper troposphere and lower stratosphere, the Raman nitrogen signal is proportional to the Rayleigh signal. This assumption of insignificant aerosol scattering was met during MOHAVE-2009. In the presence of significant aerosol scattering, the full form of the correction given in Eq. (5) would need to be used. Assuming that no significant aerosol scattering was present results in the following expression

$$w^* = w\left(1 + \zeta_1 \frac{\Delta\tau(\lambda_R, \lambda_H, r)}{w}\right) \quad (6)$$

where a new constant ζ_1 has been introduced to account for the ratio of the signal backscattered at the laser wavelength and the Raman nitrogen signal. Note also that this differential transmission term $\Delta\tau(\lambda_R, \lambda_H, r)$ differs from the earlier defined one of $\Delta\tau(\lambda_N, \lambda_H, r)$ used in Eq. (1). Equation (6) has solution of

$$w = w^* - \zeta_1 \Delta\tau(\lambda_R, \lambda_H, r) \quad (7)$$

$$\sigma_w \approx \sigma_{w^*} + \sigma_{\zeta_1} \quad (8)$$

From Eq. (7) it can be seen that, with the assumption described above, the corrected mixing ratio is calculated from the measured mixing ratio by subtracting a constant times the differential transmission profile $\Delta\tau(\lambda_R, \lambda_H, r)$. The uncertainty in the corrected

AMTD
4, 7337–7403, 2011

mixing ratio is also given, where σ_x refers to the standard deviation of the respective quantities. For this approximation, the contribution due to the differential transmission term, which typically has a relative uncertainty of less than 1 %, has been excluded. Also, although the term ζ_1 is a constant in the model there is uncertainty attributed to the determination of the value of the constant. In the analysis presented here, the uncertainty is taken to be the standard deviation of the mean differences between the corrected ALVICE profiles and the FP profiles and, as will be shown later in Sect. 7.0, is conservatively estimated to be less than 0.25 ppmv during the MOHAVE-2009 campaign.

The correction described here is generally only significant in the upper troposphere and above, a range over which the differential transmission between the laser wavelength and the water vapor wavelength due to molecular scattering changes by approximately 5 %. Therefore, the uncertainty introduced by subtracting a constant from the contaminated mixing ratio as an alternative to Eq. (7) is approximately ±2.5 %. That being the case, an alternate approximation for the corrected water vapor mixing ratio is given by

$$w = w^* - \zeta_2 \tag{9}$$

$$\sigma_w \approx \sigma_{w^*} + \sigma_{\zeta_2} \tag{10}$$

where the range dependent differential transmission term has been dropped, a new correction term, $\zeta_2 \approx \zeta_1 \Delta\tau(\lambda_R, \lambda_H, r)$, has been introduced and the uncertainty in w is similar to that given above. The three forms of the corrected mixing ratio equations derived here are compared in Sect. 5.2 after addressing the case of leakage of one of the Raman signals into the water vapor channel.

It should be noted that fluorescence is modeled here as being instantaneous. Laboratory studies of reference dyes indicate lifetimes generally of less than 10 ns (Boens et al., 2007) while studies of polycyclic aromatic hydrocarbons indicate lifetimes generally of 20–30 ns with maximum values of 36 ns (Dvorak et al., 1997). When sensed by lidar, the non-zero lifetime of the fluorescence would delay and stretch the return

AMTD
4, 7337–7403, 2011

signals. However, the correction developed here is only significant in the upper troposphere and lower stratosphere where the vertical resolution of the lidar data ranges between 900 and 1200 m. This vertical resolution corresponds to temporal bin widths between 6000 to 8000 ns. The delay in the fluorescence signal due to this lifetime is considered to be insignificant when compared with the vertical resolution of the lidar data. This is the reason that the fluorescence is modeled as being instantaneous.

5.1 Excess signal due to Raman signal leakage

A similar situation that should be considered in this context is created by an insufficient optical density in the water vapor filter at the wavelength of the Raman nitrogen (or oxygen) return. This becomes particularly important in the measurement of upper tropospheric and lower stratospheric water vapor because of the very low amount of water vapor and the relatively higher amount of molecular nitrogen. Considering that a typical LS mixing ratio might be 5 ppmv and that of molecular nitrogen ~780 000 ppmv, in order to limit the contamination due to Raman nitrogen to less than 1 % of the water vapor signal, the blocking required in the water vapor filter at the Raman nitrogen wavelength is approximately 10^7. If the filter does not have sufficient blocking of the Raman nitrogen signal, this will appear as a wet bias in the water vapor channel similar to fluorescence or bleedthrough at the laser wavelength. In this case, using a similar derivation as above, the exact correction equation is found to be

$$w = w^* - \zeta_3 \Delta\tau(\lambda_N, \lambda_H, r) \quad (11)$$

$$\sigma_w \approx \sigma_{w^*} + \sigma_{\zeta_3} \quad (12)$$

where ζ_3 represents the leakage of the water vapor filter at the Raman nitrogen wavelength. Considering now the relative magnitude of $\Delta\tau(\lambda_N, \lambda_H, r)$ and $\Delta\tau(\lambda_R, \lambda_H, r)$, the following equation pertains with an uncertainty of less than ±2.0 %

$$w = w^* - \zeta_4 \quad (13)$$

$$\sigma_w \approx \sigma_{w^*} + \sigma_{\zeta_4} \quad (14)$$

AMTD
4, 7337–7403, 2011

where, $\zeta_4 \approx \zeta_3 \Delta\tau(\lambda_N, \lambda_H, r)$. The case for leakage at the Raman oxygen signal is handled in a similar manner. The conclusion is that, to a very good approximation under most upper tropospheric and lower stratospheric conditions, excess water vapor signal due to bleedthrough of the filter (at the laser fundamental or the Raman shifted wavelengths for nitrogen or oxygen) or due to fluorescence in the telescope receiver can be corrected quite accurately by the subtraction of a constant from the mixing ratio profile.

An additional comment is that the presence of afterpulsing in the water vapor PMT, which could also manifest itelf as a wet bias in the water vapor mixing ratio, would require a different mathematical formulation since it is the intensity of the water vapor signal (as opposed to the Rayleigh-Mie one) that stimulates additional signal in the water vapor channel and the magnitude of the excess signal at a particular height in the profile is related to the total water vapor content below that altitude (Piironen, 1994).

5.2 Comparison of the correction equations

Equations (5), (7) and (9) were evaluated using several long data runs acquired during the MOHAVE-2009 campaign. ALVICE Raman lidar measurements were used on the nights of 10/20, 10/21, 10/25 and 10/27 to compare the effect of the different correction equations. On these nights there were a total of 5 FP measurements. The magnitude of the correction constants ζ_0 and ζ_1 were chosen empirically to yield best mean agreement with the FP in the 10–20 km altitude range. The mean comparison of the uncorrected lidar data and the corrected data using the three correction techniques is shown on the left side of Fig. 2. The results using Eqs. (5), (7) and (9) are referred to as "Corr1", "Corr2" and "Corr3", respectively. The two approximate corrections shown in green and blue agree within 1 % of each other and are always in agreement with the exact correction to better than 5 % (generally much better) as expected.

It would be preferred to use the exact form of the correction given by Eq. (5). This was attempted using a single hour of lidar data from the night of 10/26 and the results are shown on the right of Fig. 2. Here the signal-to-noise in the Rayleigh-Mie signal

AMTD
4, 7337–7403, 2011

averaged over 1 h is insufficient to produce a stable correction. This is due both to the generally small values of $P(\lambda_H, r)$ and the lower signal to noise in the Rayleigh-Mie data for the one hour measurements versus the all night ones shown on the left. For this reason, Eq. (7) was chosen as the preferred correction technique to use for processing the MOHAVE-2009 data.

Having determined that Eq. (7) was the preferred correction technique to use, a single value of ζ_1 was determined for the entire MOHAVE campaign using all available lidar/FP comparisons over the course of the MOHAVE campaign. All ALVICE water vapor data were corrected using this fixed value of ζ_1.

6 ALVICE lidar calibration and data products

A new technique for calibrating Raman lidar water vapor profiles with respect to radiosonde data was developed during the analysis of the MOHAVE-2009 data. Also, more detailed data files were created that provide insight into the various corrections that are applied to the data and the estimated total uncertainty budget of the data. These are described next.

6.1 Radiosonde based calibration technique

A traditional and very common method for calibrating a Raman water vapor lidar is to derive a calibration by comparison with a balloon borne radiosonde. The fact that the sonde does not sample the same atmosphere as the lidar coupled with the generally high variability of lower tropospheric water vapor, particularly at a mountain-top location like Table Mountain, raises concerns for how to best implement this technique. This question was discussed at the NDACC Raman water vapor lidar calibration workshop held in Greenbelt, MD in May 2010 and ideas for quantifying atmospheric variability of water vapor and its influence on the calibration result were generated. The algorithm used here for lidar calibration with respect to radiosonde profiles was developed as an

AMTD
4, 7337–7403, 2011

outgrowth of the discussions at the workshop. It attempts to account for the influence of atmospheric variability on a profile-by-profile basis. A flow chart of the algorithm is given in Fig. 3 and next we provide a description of how the algorithm operates.

The algorithm works on the assumption that if the lidar and the radiosonde are sampling the same atmosphere within a given range cell, the shape of the mixing ratio curves in that portion of their respective profiles will be geometrically similar. The mean proportionality constant between those geometrically similar curves will be the calibration constant derived from that portion of the profile. The algorithm proceeds over a specified range of minimum and maximum altitudes and performs a series of linear least squares and least median of squares regressions for subsets of the data within these range limits. These regressions are used to gauge the similarity of the shapes of the curves through the R^2 values of the linear regressions and to eliminate outliers through the use of the least median regressions. As implemented here, ordered pairs of lidar and radiosonde data from 0.5 km range segments are regressed within the height range of 3 and 7 km m.s.l. Ordered pairs are accepted as members of the final set of data used to determine the calibration value if, first, they were part of a regression with sufficiently high R^2 and, second, if an individual ordered pair is within a certain percentage of a least median of squares fit line. The algorithm is adaptive so that if after the first pass through the profile an insufficient number of points has qualified for the calibration determination, the acceptance criteria for R^2 and maximum deviation from least median of squares prediction line are relaxed and the process is repeated until the desired number of ordered pairs is obtained. The final calibration value is determined by the mean ratio of the lidar and radiosonde data and not by the slope of a regression line.

An example of the results of this routine is shown in Fig. 4 using a radiosonde comparison on the night of 21 October 2009. The plot in the upper left shows the radiosonde and lidar profiles in the region of interest. The calibration constant derived by the algorithm for this comparison has been used here for scaling the lidar data. In the upper right are plotted just the ordered pairs that were finally accepted by the algorithm

AMTD
4, 7337–7403, 2011

for use in determining the calibration constant. Here the ability to select the parts of the profile that show similar geometrical shapes is demonstrated. In the lower left is shown a comparison of the linear regression of all points within the 3 to 7 km range (in black) along with only the qualifying points used in the calibration determination. In this plot also can be found the calibration constants calculated with both the full population of points before any selection (yielding a value of 114.92 g kg^{-1}) and just those that qualified after selection (117.86 g kg^{-1}). For these examples, the minimum number of order pairs required to perform the calibration was set at 30. This corresponds to a range in the atmosphere of 900 m.

A study of the calibration constants derived using this technique indicated that the standard deviation of the constants decreased as the minimum acceptable R^2 value required to obtain 30 ordered pairs increased. This implies that the more geometrically similar the lidar and radiosonde profiles are, the more stable the derived calibration constant. It was also found that restricting the RH values from radiosonde to values above 5 % RH further decreased the standard deviation of the derived constants. Low RH conditions are known to cause the absolute errors in Vaisala RS92 RH data to increase (Miloshevich et al., 2009) and are best avoided for use in lidar calibration. Considering the indication that the corrections applied to the Vaisala RS92 data may have over-corrected during MOHAVE-2009 (c.f. Appendix A), the final calibration value used for the processing of the ALVICE Raman lidar data was determined by averaging the calibration constants determined from corrected RS92 and frostpoint hygrometer (FP). The two calibration constants differed by approximately 5 %. This averaging was done to compensate for the dry bias of the corrected RS92 data compared with frost-point hygrometer shown in Fig. 12.

Prior to data runs on 10 nights during MOHAVE-2009, a stabilized tungsten lamp was used to directly illuminate the lidar receiver in an implementation of the “hybrid technique” (Leblanc and McDermid, 2008, 2011a; Whiteman et al., 2011a). The ratio of the signals in the water vapor and nitrogen channels due to the lamp illumination is recorded with the goal of using this ratio to stabilize the calibration obtained from

AMTD
4, 7337–7403, 2011

radiosonde. The standard deviation of radiosonde-derived calibration constants was 5.5 % without implementing the hybrid technique and was 5.6 % by implementing the hybrid technique. Thus, no improvement in calibration stability was achieved by use of the recorded lamp ratios. The lamp ratios recorded during the first 5 nights of operation showed a standard deviation of approximately 5 % while the lamp ratios for the remaining 5 nights showed a standard deviation of less than 1 %. Comparison of ALVICE water vapor profiles with those of the other lidars and balloon-borne sensors do not indicate that the calibration constant of the lidar was truly more variable during the early part of the mission versus the latter. Therefore, we speculate that the considerably higher standard deviation during the first 5 nights may have been due to slight shifting of position of some of the residual insect material at the location on the telescope primary mirror that is being sampled by a single, fixed calibration lamp as implemented during MOHAVE-2009 (Whiteman et al., 2011a). Since that time, the ability to scan the full telescope aperture with the calibration lamp (Venable et al., 2011) has been added to the ALVICE system.

6.2 ALVICE Raman water vapor lidar data products

A lidar datafile was created corresponding to the time of each radiosonde launch that occurred during operations of the ALVICE Raman lidar. In this datafile are several versions of water vapor mixing ratio profiles and ancillary data that will be discussed in the upcoming analysis. The Guide to the Expression of Uncertainty in Measurements (JCGM/GUM, 2008) states that "In practice, the required specification or definition of the measurand is dictated by the required accuracy of measurement. The measurand should be defined with sufficient completeness with respect to the required accuracy so that for all practical purposes associated with the measurement its value is unique." Given that there are various studies in which the water vapor profile data supplied here may be used (e.g. trend detection in the UT, trend detection in the LS, satellite retrieval validation, satellite radiance validation) and the accuracy needed in the water vapor

AMTD
4, 7337–7403, 2011

profile differs for each type of study, we attempt to provide in these datafiles an estimate of the total uncertainty due to all significant influence factors. The usefulness of an individual profile is then determined by considering the total uncertainty of the profiles as a function of altitude and the tolerance for uncertainty of the specific scientific study desired.

Thus, for all versions of the ALVICE data analyzed for the MOHAVE campaign, the total uncertainty is estimated by including the following contributions:

1. Uncertainty due to random error in the lidar data calculated assuming Poisson statistics.
2. Uncertainty in the correction for the lidar overlap function which is as large as 10 % in the lowest levels of the atmosphere.
3. Uncertainty of the calibration source. Based on absolute accuracy information found in Miloshevich et al. (2009) and Vömel et al. (2007b) the accuracy of the calibration sources vary between 4 % in the lower troposphere to 10 % in the lower stratosphere.
4. Uncertainty in the transfer of the calibration source to the lidar profile, which is estimated at 1–2 %.
5. Uncertainty in the correction for the temperature dependence of Raman scattering, which is estimated to be less than 1 %.
6. Uncertainty in the correction for differential transmission of the atmosphere at the two Raman wavelengths, which is estimated to be less than 1 %.
7. Uncertainty in the correction for fluorescence. The correction for fluorescence is determined in Sect. 7.0 to be essentially constant during the campaign. To be conservative, an uncertainty of 0.25 ppmv was used in the data files.

AMTD
4, 7337–7403, 2011

The datafiles include water vapor mixing ratio profiles with different temporal resolution. The spatial resolution of all the profiles except the raw data profile is determined by the size of a moving window filter which varied from 30 m in the lowest part of the atmosphere to a maximum of 1200 m for ranges beyond 12 km. The three different vertically smoothed data products contained in the datafiles are

1. a one hour summation beginning at the time of the radiosonde launch, independent of altitude.
2. all available data for a given night, independent of altitude.
3. variable temporal and spatial smoothing to limit the random error, if possible, to less than 5 %.

There are 4 corrections that are applied to all water vapor profiles in these datafiles and the values of these corrections are given individually in the datafiles. The corrections are for water vapor mixing ratio overlap dependence, temperature dependence of Raman scattering, atmospheric differential transmission and the signal dependent correction that is described in Sect. 5.

The 3 processing methods listed above have been studied previously (Whiteman et al., 2006c) and method 3 has proven to be preferred for satellite validation because of its ability to capture the high variability of lower tropospheric water vapor. Therefore, for MOHAVE-2009, an additional data product referred to as the "best estimate" product was created. Borrowing from the philosophy of the DOE/ARM program (Ackerman and Stokes, 2003; Tobin et al., 2006) whereby the best available data are supplied as a function of altitude, the ALVICE best estimate profile is comprised of the 3 profiles listed above, including all corrections, along with a surface reference point derived from the surface reference data shown in Fig. 1. This best estimate product is intended to be the most accurate profile of atmospheric water vapor at the time of the radiosonde launch from the ALVICE lidar perspective. An illustration of this is provided in Fig. 5. On the left is shown a single profile comparison of the ALVICE best estimate profile, 1 h

AMTD
4, 7337–7403, 2011

sum profile and all night profiles for the radiosonde launch on 25 October at 03:55 UT. There was a large gradient in water vapor near the surface that filled in as time passed so that the best estimate product, which used as little as two minutes of data in the composite profile in the lower atmosphere, was able to capture this dry feature. The 1 h and all night sums show large differences from the sonde. The mean bias and RMS for 33 Vaisala RS92 and ALVICE best estimate, 1 h and all night profile comparisons are shown in the middle and on the right of Fig. 5. The RMS difference between sonde and best estimate product is consistently less than the 1 h and all night averages up to an altitude of approximately 7 km. The mean RMS for the best estimate, 1 h and all night averages up to an altitude of 7 km are respectively 17 %, 22 % and 50 %. The mean biases for the three different ALVICE profile products are 1.3 %, 2.5 % and 25 %. Thus, for the entire MOHAVE-2009 campaign both in terms of RMS and bias, the technique of using variable temporal averaging is found to agree better with radiosonde below 7 km. The small tendency for the 1 h data to show lower RMS and bias than the best estimate product above 6–7 km may be an indication that the averaging time used in the best estimate product in this altitude range should be increased. These results indicate that, in general, the best estimate profile provides a better representation of the state of the atmosphere at the time of the radiosonde launch than either the 1 h or all night profiles. The large mean bias of the all night data shown on the right of the figure implies that cases such as that illustrated on the left of the figure where a dry layer filled in over the night occurred with some frequency during MOHAVE-2009 and that care should be taken in comparing extended averages of lidar data with sensors that measure more rapidly such as those carried by radiosonde or satellite.

7 Comparisons of lidar profile and total column water vapor measurements

Comparisons of the fully processed water vapor profiles from the ALVICE Raman lidar were made with respect to RS92 and FP. The mean normalized differences of the 1 h

AMTD
4, 7337–7403, 2011

lidar summed profiles were formed with respect to Vaisala RS92 and FP. The mean normalized difference of the "all night" summed ALVICE lidar profiles were also formed with respect to FP. These three comparisons are shown in Fig. 6. There were 19 comparisons of ALVICE lidar and RS92 and 11 comparisons of ALVICE lidar and FP. The 1 h plot versus RS92 shows a moist bias of the lidar of approximately 20 % in the lowest 0.5 km. The study of radiosonde profile similarity performed in Sect. 6.1 indicates that some of this bias is due to a persistent tendency for the atmospheric layer directly above the mountaintop lidar site to be moister than the layer immediately downwind of the site, where the radiosonde sampled. Above this surface layer, the ALVICE lidar 1 h profiles agree with the RS92 within 10–15 % up to an altitude of 14 km with the radiosonde profiles showing a tendency to become increasingly dry of the lidar profiles for altitudes above approximately 8 km. The analysis of RS92 and FP data shown in Appendix A also indicates that the corrected RS92 becomes increasingly dry of the FP with increasing altitude consistent with the relative behavior of the lidar and RS92 profiles. The differences between RS92 and FP or lidar are within the uncertainty of the Vaisala correction algorithm but further support the possibility that the RS92 calibration may have changed since the time the RS92 correction algorithm was determined. These points are further discussed in Appendix A.

The comparison of 1 h lidar profiles and the frostpoint measurements shows generally more scatter than the comparison versus the RS92 due to the reduced statistics. The feature in the range of 10–11 km that shows a large positive bias of approximately 30 % is due to a small number of cases where the atmospheric profile of water vapor showed a rapid decrease above 10 km. The ALVICE data processing used a vertical smoothing in this region with vertical resolution of approximately 0.5 km which created significant differences with the FP which showed rapid decreases in the water vapor concentration over ranges shorter than 0.5 km.

The comparison of all night lidar profiles and FP used the same 11 FP launches as in the 1 h comparsons. The tendency for the all night lidar profiles to exhibit a moist bias already mentioned with respect to Fig. 5 is evident here as well. Below approximately

AMTD
4, 7337–7403, 2011

12 km, the lidar profiles are wetter than the FP profiles by approximately 10 % discounting the regions of high atmospheric variability at altitudes of approximately 4, 8 and 11 km where deviations were higher. These differences are believed to be mainly due to a tendency for the atmospheric conditions over the mountain top site to moisten during the night and not due to real instrument measurement differences. Above 12 km, where the measurements of FP may be expected to generally be more representative of the all night lidar measurements the comparisons improve considerably with ALVICE lidar agreeing with FP within generally better than 10 % to beyond 18 km.

The question of whether there was significant variation in the value of the correction factor, ζ_1, during the MOHAVE mission can be addressed with the aid of Fig. 6 where the standard deviation of the comparisons of all FP and all night summation lidar comparisons is plotted above 14 km. Consider that the displayed standard deviations of the normalized differences between corrected ALVICE and FP range between approximately 10% and 15%. The standard deviation of the lidar data alone ranged from 8% to 15% in this altitude range, while the accuracy of the FP is given as 10% in this part of its profile. There is also variability contributed by the spatio-temporal mis-match between lidar and FP measurements as well as potentially by variation in the correction factor. But the entire standard deviation budget is likely accounted for by considering only the variability in the lidar and the FP without considering any contribution due to spatio-temporal mismatch or variation in the correction factor. It seems reasonable to state, therefore, that there is no evidence for significant day-to-day variability in the correction factor, ζ_1. This result indicates that the use of an optical window over the lidar telescope augmented by a large capacity fan and daily window washings may be sufficient measures for preventing the accumulation of fluorescing material on a Raman lidar system.

7.1 Total column water comparisons using GPS, radiosonde and lidar

A more detailed comparison of the total column water measurements made during MOHAVE-2009 is performed in (Leblanc et al., 2011b). Therefore, here we give just

AMTD
4, 7337–7403, 2011

a brief description of the measurements made by the GPS system that accompanies the ALVICE trailer on its mobile deployments. This system is the only "rover" within the international SuomiNet network (Ware et al., 2000). It has been used previously as the calibration source for mobile Raman lidar water vapor measurements made during the International Water Vapor Project (IHOP) campaign held in the mid-west US in 2002 (Whiteman et al., 2006a,b) using a similar calibration procedure as that developed within the DOE/ARM program (Turner et al., 2002). During IHOP, comparisons made between lidar and frostpoint hygrometer (Whiteman et al., 2006a) and airborne water vapor lidars (Behrendt et al., 2007) showed agreement of calibration to generally better than 10 %.

During MOHAVE-2009, the SuomiNet GPS system with ID SA65 operated continuously from 10 October through most of 27 October 2009. The integrated precipitable water and pressure data from SA65 were combined with the temperature and RH data from the THPref instrument to provide a surface reference datafile containing RH, T, P, IPW and water vapor mixing ratio with a 5 min temporal resolution for the period 10–27 October as previously shown in Fig. 1.

In general, Raman lidar systems have difficulty with measurements at close ranges due to the influence of the lidar system overlap function (Harms et al., 1978). This can be seen to varying degrees in the Raman lidar data archived for MOHAVE-2009. A correction has been applied to the ALVICE Raman lidar data for these near field effects. By carefully selecting radiosonde profiles in a manner similar to that described in Sect. 6.1, an overlap correction was derived as the mean ratio of radiosonde and lidar data for the selected profiles. This technique has been used successfully previously (Turner et al., 2002; Whiteman et al., 2006c). The correction extends from the first reported lidar range bin which is generally at 60 m a.g.l. to 1.2 km a.g.l. and reaches a maximum of ~40 % at the closest ranges. The combination of overlap-corrected lidar mixing ratio extending down to 60 m along with a ground point derived from the ALVICE surface reference data improves the IPW calculated from lidar.

AMTD
4, 7337–7403, 2011

The IPW from SA65 and RS92 radiosonde were compared with the integrated precipitable water calculated from the best estimate ALVICE Raman lidar water vapor mixing ratio profile. The results are shown in Fig. 7. The mean ratio of IPW derived from lidar and IPW from RS92 and GPS, respectively, were found to be 1.04 and 1.05 indicating that the lidar was approximately 5 % moister than either of these instruments. This moistness with respect to the corrected RS92 is consistent with the dryness of the corrected RS92 versus FP shown in Fig. 12 making the ALVICE lidar results in better agreement with those of FP in the lower troposphere.

8 Wet Biases during the MOHAVE campaigns

Without application of the signal-dependent correction described in Sect. 5, the ALVICE water vapor measurements possessed a significant moist bias in the upper troposphere as shown in Fig 2. Previous experiments at Table Mountain both prior to and including the MOHAVE-2009 experiments have also demonstrated moist biases in the upper troposphere lidar measurements (Leblanc et al., 2007). In 2006, the NASA/GSFC Scanning Raman and Aerosol Temperature (AT) lidars were transported to Table Mountain for comparisons with the Table Mountain Raman lidar during MOHAVE-I. The main SRL lidar telescope was severely damaged during transportation for this mission but an ancillary fiber-coupled receiver (Whiteman et al., 2006a) intended for the low-altitude SRL measurements was used during the campaign. The water vapor measurements made with the SRL small telescope and those of the AT and JPL lidars all showed wet biases in the upper troposphere. The wet biases were attributed to fluorescence in fiber optics in the case of the SRL ancillary telescope and the JPL system. Following MOHAVE-I, in order to address the wet biases observed, the JPL and AT systems were upgraded to reduce fluorescence contamination. The SRL system was de-commissioned due to the damage sustained and the airborne RASL instrument was installed in the same trailer that had contained the SRL instrument and used in an upward-looking configuration (Whiteman et al., 2010). These lidar systems participated in MOHAVE-II in 2007. The final analysis of MOHAVE-II data showed small wet biases of 0.5–2.0 ppmv remaining

AMTD
4, 7337–7403, 2011

in the ALVICE and JPL lidar measurements in the 16–18 km range. The AT system likewise exhibited a moist bias in the upper troposphere. Further equipment modifications were made following MOHAVE-II and MOHAVE-2009 was staged to test again whether fluorescence had been eliminated from the receiver optics of the three lidar systems. In anticipation of MOHAVE-2009, the TMW system from JPL (McDermid et al., 2011a) was converted from a fiber coupled system to a direct coupled one. Optical glass designed to reject laser light at 355 nm was used in both the AT and ALVICE lidar systems. Unfortunately, laser problems prevented the AT system from participating significantly in the MOHAVE-2009 campaign. An additional lidar from NASA/GSFC, the STROZ-LITE (Stratospheric ozone lidar trailer experiment) (Stiller et al., 2011) also participated in MOHAVE-2009.

Between MOHAVE-II and MOHAVE-2009, the ALVICE instrument participated in the WAVES_2009 campaign held at Beltsville, MD. As mentioned before, no moist bias was observed in the ALVICE measurements when compared with the frostpoint hygrometer during WAVES_2009 indicating that all significant sources of fluorescence had been eliminated from the lidar receiver optics. Thus, the expectation was that the ALVICE lidar would agree well with the FP measurements during MOHAVE-2009. The insect contamination that occurred on 16 October is believed to have led to the different result that was obtained, however.

The data acquired by all three lidar systems during MOHAVE-2009 have undergone various versions of processing. At various points during this process all three Raman lidars exhibited significant wet UT biases of differing magnitudes. The techniques employed to address these wet biases differed among the three lidar systems. For the STROZ system a blocking filter was used to reject 355 nm light from entering the receiver optics greatly reducing the potential for fluorescence in the receiver optics and significantly reducing the wet bias. For the TMW system, the wet bias was removed by increasing the width of the digital smoothing filter. For the case of the ALVICE Raman lidar, the correction for signal dependent contamination derived in Sect. 6 was applied to the data to address the wet bias.

AMTD
4, 7337–7403, 2011

9 Quality control of upper tropospheric Raman water vapor lidar measurements

Global climate models indicate that upper tropospheric water vapor is anticipated to increase significantly during the current century (Held and Soden, 2006; Soden et al., 2005; Oman et al., 2008; Boers and Meijgaard, 2009; Whiteman et al., 2011b). Water vapor mixing ratio increases of up to 1 % per year or higher are predicted by these models with the largest trends anticipated in the tropical upper troposphere at the 150–250 hPa levels (Soden et al., 2005; Boers and Meijgaard, 2009; Whiteman et al., 2011b). Furthermore, recent studies indicate that these same pressure levels may be the most efficient ones for monitoring long term trends (Boers and Meijgaard, 2009; Whiteman et al., 2011b). By contrast, lower stratospheric water vapor is anticipated to increase less (Oman et al., 2008; Whiteman et al., 2011b). The variability in stratospheric water vapor is also substantially lower than in the upper troposphere as evidenced by the 30-yr Boulder time series from NOAA FPH (Hurst et al., 2011a). This implies that monitoring trends in the lower stratosphere requires much more accurate measurements than in the upper troposphere (Whiteman et al., 2011b) where random uncertainties of 50 % and more appear tolerable. It also implies that additional noise or imperfections in the data record due to increases in random error, data gaps or biases will have a more significant effect on the time to detect trends in the lower stratosphere than in the upper troposphere. The error budget of a Raman lidar system increases with altitude so that the errors are significantly larger in the LS than in the UT implying that it may be more practical to consider Raman lidar for monitoring trends in the UT than the LS. The potential for wet biases being a larger fractional contamination in the LS than in the UT strengthens the argument that the focus of Raman water vapor lidar trend monitoring efforts should be in the UT and not the LS. Still the lower stratospheric water vapor measurements of those Raman lidar systems able to measure that high into the atmosphere can be useful both for quality control of the data as well as a source of correction that improves the upper tropospheric water vapor measurements potentially making them suitable for water vapor trend monitoring studies.

AMTD
4, 7337–7403, 2011

Consider Fig. 8 which presents the monthly average water vapor mixing ratios over Table Mountain, CA as measured by the Microwave Limb Sounder (MLS) using v3.3 data from August, 2004 to February, 2011. The value plotted is the mean water vapor mixing ratio within the height range of 17 km to 19.6 km. For the MLS data, geopotential altitudes are used. They differ by less than 1 % from the geometrical altitude in this height range. The number of retrievals averaged over the 7-yr period is plotted with a dashed line. The 2-σ error bars plotted cover approximately 95 % of the number of cases. Thus, 95 % of the measurements at Table Mountain over this period of 7 yr fall within the range shown by the error bars on this plot. The absolute accuracy of MLS water vapor measurements at approximately 150 hPa is given (Livesey et al., 2011) as approximately 15 % with single-profile MLS precision reported as 0.2–0.3 ppmv (Lambert et al., 2007). Comparisons of MLS with CFH (Vömel et al., 2007b) above the tropical tropopause show agreement within 2–6 %. If we take, then, the results in Fig. 8 to represent a current climatology of lower stratospheric water vapor over Table Mountain accurate at the 5–15 % level, we can use it as a means to quality control Raman water vapor lidar data. For example, if Raman lidar LS measurements fall outside of the mean $\pm 2\sigma$ values shown in Fig. 8, then there is a 95 % likelihood that the Raman lidar data are biased in the lower stratosphere. This determination can be used as a source of correction to the data following the guidelines of the GUM (JCGM/GUM, 2008) where systematic biases are assumed to be corrected for. Recalling the many years of Raman lidar data described in Sect. 4.4 that indicate lower stratospheric water vapor mixing ratios outside of a reasonable range of values, this technique could also provide a way to correct those data. We will now test this concept on the ALVICE Raman lidar data and compare with the correction achieved by comparison with actual frostpoint measurements during the MOHAVE-2009 campaign.

During the MOHAVE-2009 campaign 11 frostpoint hygrometer ascents (Hurst et al., 2011b) were available for direct comparison with the ALVICE lidar profiles. This permitted the calculation of a correction value, ζ_1, in Eq. (7) that gave good agreement with the mean frostpoint measurements in the altitude range of 10–20 km. As stated

AMTD
4, 7337–7403, 2011

earlier we believe the dominant cause of the wet bias present in the ALVICE lidar measurements to be fluorescence from insect material that was deposited on the telescope mirror early in the MOHAVE-2009 campaign. The value of $\zeta_1 \Delta\tau(\lambda_R, \lambda_H, r)$, therefore, can be considered to be a best estimate of the excess water vapor signal due to fluorescence from insect contamination for the configuration of the lidar during MOHAVE-2009. The difference between the mean lidar measurement and the MLS climatology can also be used to define ζ_1 or ζ_2 in Eqs. (7) and (9), respectively. Correction to a reasonable mean value in the LS would provide corrected data extending down into the upper troposphere where (1) trend detection is less influenced by additional noise sources and thus easier to perform, and (2) water vapor mixing ratios are much higher thus decreasing the relative measurement uncertainty of Raman lidar systems and the magnitude of the influence of the assumption of the mean LS water vapor mixing ratio.

We now will use the MLS climatology shown in Fig. 8 to calculate the wet bias correction value, ζ_1, and compare the results with the value calculated from direct comparison with the frostpoint reference measurements made during MOHAVE-2009. The mean mixing ratio measured by frostpoint during MOHAVE-2009 between the altitude ranges of 17.0 km and 19.6 km was approximately 4.7 ppmv which is in very good agreement with the MLS mean climatology shown in Fig. 8. Determining the correction value, ζ_1, for the ALVICE lidar from the MLS climatology between the altitude ranges of 17.0 km and 19.6 km, which is above the tropopause where the MLS data have known biases (Livesey et al., 2011), yields a value of ζ_1 that is approximately 0.3 ppmv larger than the value achieved through comparison with frostpoint hygrometer between the ranges of 10 km to 20 km. ALVICE profiles using these two values of ζ_1 in Eq. (7) are included in Fig. 9.

On the left of the figure is shown the mean profiles for all available data during MOHAVE-2009 for FP, MLS and the ALVICE lidar where both best estimate data and those corrected using the MLS climatology discussed above are shown. The MLS vertical resolution in this altitude range is approximately 2.5 km to 3.1 km (Livesey et al., 2011). For altitudes above 12 km, the ALVICE lidar profiles possess vertical resolution

AMTD
4, 7337–7403, 2011

of approximately 0.5–0.75 km using the Verein Deutscher Ingeneure (VDI4210, 1999) definition of vertical resolution for lidar systems. All profiles generally reveal similar features except for the departure of the MLS profile from the others below an altitude of approximately 14 km. Biases and deviations are better revealed by the plot on the right which shows the normalized difference of MLS, ALVICE (both best estimate and with correction derived from MLS climatology) with the FP profiles. MLS agrees with frostpoint hygrometer within generally better than 10 % above an altitude of 14 km. The previously mentioned upper tropospheric dry bias in MLS is evident below this altitude reaching a maximum of approximately 40 % at an altitude of 12 km. The two versions of ALVICE profiles agree within 10 % of the frostpoint from 10 km to 20 km.

Figure 9 indicates that similar results are obtained in the ALVICE data if MLS climatology is used to derive the signal dependent bias correction for use in Eq. (7) instead of the actual frostpoint measurements made during MOHAVE-2009. This should not be surprising given the fact that the MOHAVE-2009 mission took place during more than half of the month of October and there were good statistics for UTLS measurements from both FP and ALVICE lidar during that period. Thus, the measurements made during MOHAVE-2009 are likely to represent a reasonable mean value for the month of October.

As mentioned, recent results (Whiteman et al., 2011b) indicate that the most efficient level in the atmosphere for revealing trends in the atmospheric water vapor mixing ratios in the mid-latitudes may be approximately 200 hPa. During MOHAVE-2009 this pressure level corresponded roughly with the 12 km altitude level. The mean mixing ratio measured by frostpoint hygrometer at 12 km during MOHAVE-2009 was approximately 32 ppmv. Recall also Eq. (9) that indicates that a signal dependent bias in Raman water vapor lidar measurements manifests itself as nearly a constant bias in mixing ratio space. Taking the 2-σ value of 1.3 ppmv from Fig. 8 as the uncertainty in the mean value of the lower stratospheric mixing ratio of water vapor during the MOHAVE-2009 campaign and taking the conservative value of 0.25 ppmv used in the ALVICE lidar datafiles (cf. Sect. 6.2) as the uncertainty in the determination of the bias

AMTD
4, 7337–7403, 2011

correction, ζ_1, and considering as well the uncertainty of the mean MLS value shown in Fig. 8 to be approximately 0.5 ppmv, the propagated uncertainty of the correction becomes approximately 1.4 ppmv. Under the conditions present during the MOHAVE-2009 campaign, therefore, the use of MLS climatology to correct Raman water vapor lidar bias would contribute an additional uncertainty of approximately 4 % to the Raman lidar measurement of water vapor at the 200 hPa level in the upper troposphere, a region of the atmosphere where recent research (Whiteman et al., 2011b) indicates that random uncertainties of 50 % and more are acceptable for trend detection purposes.

10 Discussion

One of the goals of the NDACC Raman water vapor lidar effort is that of trend monitoring of water vapor in the atmosphere. Trends in lower stratospheric water vapor are clearly important in atmospheric science. For example, Solomon et al. (2010) recently showed that the 10 % decrease in stratospheric water vapor amounts that occurred after the year 2000 acted to slow the rate of increase in global surface temperature over the period 2000–2009 by about 25 % compared to that which would have occurred due only to carbon dioxide and other greenhouse gases. However, as mentioned earlier models predict that mean upper tropospheric water vapor mixing ratios are predicted to increase by up to 100 % or more over the coming century due to surface temperature increases while mean lower stratospheric mixing ratio increases are anticipated to be less than half that amount (Soden et al., 2005; Boers and Meijgaard, 2009; Whiteman et al., 2011b). Existing studies indicate that the region of the atmosphere where trend detection is most resistant to additional noise in the water vapor measurements and thus could be easier to perform is the upper troposphere and not the lower stratosphere (Whiteman et al., 2011b) and it needs to be noted that the random errors in Raman lidar data in general increase rapidly progressing from the upper troposphere into the lower stratosphere.

AMTD
4, 7337–7403, 2011

There are additional factors that are of concern when considering the possibility of developing a climate quality data record of lower stratospheric water vapor from Raman lidar. NDACC Raman lidars typically operate open to the atmosphere. The possibility of contamination of optics by fluorescence inducing insects (Byrdegaard et al., 2009) or pollen (Saito et al., 2010), for example, or the possibility that airborne fluorescing particles (Gelbwachs and Birnbaum, 1973; Pan et al., 1999; Pinnick et al., 2004; Immler et al., 2005) or degraded hardware (Piironen, 1994) are biasing the data must be considered in developing procedures for data quality control. These biases can be significant with respect to the mean LS water vapor mixing ratio. The possibility for system dependent biases to be present within the NDACC Raman lidar network is increased by the fact that each instrument within the network is unique both in terms of its hardware and software.

Therefore, considering the low signal-to-noise of the Raman lidar measurements in the lower stratosphere, the documented tendency for various factors to lead to generally wet biases in the measurements, and the need for higher accuracy measurements for trend detection in the lower stratosphere than the upper troposphere (Whiteman et al., 2011b), it seems more practical to target upper tropospheric water vapor as the prime measurement goal for Raman lidars. This can be aided by putting in place quality control procedures that can be used to check for the presence of biases in Raman lidar water vapor data on a regular basis and correct them.

With optimization, in particular through decreasing the noise due to skylight and from the detector itself, the measurements here and elsewhere (Whiteman et al., 2010; Leblanc et al., 2011b) demonstrate that Raman water vapor lidars can have significant sensitivity to water vapor in the lower stratosphere although those measurements may be influenced by the biases mentioned earlier (cf. Sect. 4). The above details create the context for the proposed quality control procedure based on lower stratospheric water vapor climatology that may also be used for correction of data that possess signal dependent bias. Given that biases could develop at any time due, for example, to deposition of material or degradation of system hardware, on-going tests for the presence of

AMTD
4, 7337–7403, 2011

biases should be performed. The procedure outlined here can be implemented without the need for a validation campaign involving FP launches and could be implemented routinely by Raman water vapor lidar systems within NDACC.

As mentioned before, recent work indicates that the tolerance for water vapor measurement uncertainty is rather high when considering the task of trend detection in the upper troposphere. But it is important for all components of the uncertainty budget to randomize over time (Whiteman et al., 2011b). The correction procedure described here, if implemented regularly as a part of the data processing protocol, would accomplish that for signal-dependent biases in the water vapor lidar measurements and thus help to normalize the upper tropospheric measurements across the NDACC network.

The need for data quality control in climate data records is illustrated by the efforts relating to quantifying atmospheric temperature trends using radiosondes. The historical record of radiosonde temperatures is plagued by various data quality issues (Seidel et al., 2004). A workshop convened to compare different data harmonization techniques concluded that the various techniques yielded sufficiently dissimilar results that no conclusions could be drawn as to the best method for adjusting the time series (Free et al., 2002). The point to be taken from this history is that, despite best intentions, errors do arise in data series that are intended to last for a period of decades and that data quality control measures should be implemented at the initiation of a data record intended for climate monitoring purposes.

The use of mean lower stratospheric water vapor climatology as quality control and as a source of "tie point" for correcting upper tropospheric water vapor measurements over an extended period of time relies on future knowledge of LS water vapor mixing ratios. These values are anticipated to increase from current mid-latitude values of approximately 3–6 ppmv to perhaps 5–9 ppmv over the coming century (Oman et al., 2008; Whiteman et al., 2011b) while the anticipated changes in UT water vapor mixing ratio at the 200 hPa level may increase from the ~30 ppmv measured during MOHAVE-2009 to 60 ppmv or greater over the same period of time. Since future UT water vapor mixing ratios are expected to increase more than those in the LS, it is

AMTD
4, 7337–7403, 2011

possible that the added uncertainty of using LS water vapor mixing ratio as a "tie point" for data correction will contribute a smaller amount to the uncertainty budget in the future than was the case here where it amounted to an estimated 4 % at 200 hPa. Therefore, the future uncertainty of LS water vapor mixing ratios is not anticipated to diminish the utility of using mean LS values for quality controlling and correcting future Raman lidar upper tropospheric data.

11 Summary and conclusions

The participation of the mobile system known as ALVICE in the MOHAVE-2009 field campaign has been described. The ALVICE system deployed to Table Mountain, CA for MOHAVE-2009 with a large suite of remote sensing and in-situ instrumentation for quantifying water vapor and other atmospheric constituents. The time series of ancillary measurements is shown in Fig. 1. The measurements from the surface reference system called THPref and frostpoint hygrometer were used to characterize the accuracy of uncorrected and corrected Vaisala RS92 data acquired during MOHAVE-2009. The estimated total uncertainty for corrected RS92 measurements during the MOHAVE-2009 campaign were ±(5 % + 0.5 % RH) for RH > 10 % and ±(7 % + 0.5 % RH) for RH≤10 %, which corresponds to an uncertainty of ±6 % at 50 % RH, ±10 % at 10 % RH, and ±24 % at 3 % RH. The comparison to FP shown in the appendix is consistent with this uncertainty estimate, but still there is evidence that the calibration correction documented in Miloshevich et al. (2009) is less accurate for 2009 radiosondes than for 2006–2007 radiosondes, the vintage of sensor used to develop the correction, due to expected changes in the RS92 mean bias with time, indicating that the uncertainty estimate is conservative.

A new radiosonde based calibration algorithm was presented that attempts to account for the influence of the spatio-temporal mismatch between lidar and radiosonde profiles. The routine is based on the assumption that profiles of radiosonde and lidar that are sampling the same atmosphere should have geometrically similar shapes. Use

AMTD
4, 7337–7403, 2011

of this procedure was found to reduce the variability in the derived calibration constant. It was also found that avoiding portions of the profile where RH < 5 %, a region where radiosonde errors are known to increase significantly (Miloshevich et al., 2009), further reduced the variability in the derived calibration constant.

The research indicates that the ALVICE Raman lidar arrived for the MOHAVE-2009 field campaign free of any significant fluorescence. However, insects contaminated the ALVICE Raman lidar receiver early in the MOHAVE-2009 campaign and are the suspected cause of fluorescence in the lidar receiver which produced a wet bias in the ALVICE upper level measurements. Following this event, an optical window was installed over the lidar telescope, a large capacity fan was used to blow across the window during measurement periods and the window was washed daily. Given that analysis of the data indicates that the fluorescence contamination was essentially constant during the remainder of MOHAVE, it is possible that these measures are sufficient to prevent contamination of Raman water vapor lidar systems by fluorescing airborne material.

During both MOHAVE-I (held in 2006) and MOHAVE-II (2007), all participating Raman lidars exhibited wet biases in the upper troposphere. Various experimental and algorithmic modifications were made to all the lidar systems prior to MOHAVE-2009. During MOHAVE-2009, all three participating Raman lidars exhibited significant moist biases at some point in the various versions of data processing. The methods used to address these wet biases in the lidar systems varied but all were successful in reducing or eliminating the moist biases observed in the MOHAVE-2009 campaigns. Nonetheless, the conclusion at the end of MOHAVE-2009 was that two of the three participating Raman lidar systems exhibited some degree of signal dependent bias that produced an artificially wet retrieval in the upper troposphere and lower stratosphere.

Wet biases in upper tropospheric Raman lidar water vapor measurements are found to be rather common. The analysis of selections from 25 yr of data from 3 Raman lidars that did not participate in MOHAVE-2009 indicated persistent wet biases in the upper tropospheric water vapor measurements of each of them.

AMTD
4, 7337–7403, 2011

A mathematical model describing the physical process of signal dependent bias was derived and applied to the ALVICE data to correct for the observed wet bias. Applying the wet bias correction derived here, using either actual measurements by FP or lower stratospheric climatology, resulted in corrected ALVICE profiles that agreed in the mean with FP to within 10 % from 10–20 km.

The MOHAVE and WAVES experiments have shown that the elimination of all significant fluorescence from a Raman water vapor lidar system is possible through careful experimentation. However, each NDACC Raman lidar system is unique and uses custom developed algorithms therefore it should be expected that new challenges will emerge when the data from these systems receive careful inspection. How much effort will be required at these other sites to fully eliminate any wet bias that might be found? What is the likelihood that problems such as contamination by insects or pollen or degradation of hardware might create a wet bias following a cal/val campaign as may have happened with the DOE/ARM lidar in the period 1998–2003? What are the chances that fluorescence of airborne particles (Gelbwachs and Birnbaum, 1973; Pan et al., 1999; Pinnick et al., 2004; Immler et al., 2005) or signal-induced noise (Piironen, 1994) might contaminate the data in ways that may not be correctable?

Consideration of these questions and the history of the difficulty in harmonizing temperature data records (Free et al., 2002) indicates that data qualify controls should be developed within the NDACC Raman water vapor lidar effort now and put in place before data are archived for scientific use. Furthermore, archiving the complete raw data record should be considered a requirement since it would permit re-processing in the future if problems are found to have developed in the time series.

We have demonstrated a potential quality control procedure for Raman water vapor lidar measurements of UTLS water vapor. It makes use of the climatology of lower stratospheric water vapor where, at certain altitudes reachable by optimized Raman lidars, mixing ratios are found to lie within a small range of values. For Raman lidar systems that have sufficient sensitivity to reach lower stratospheric altitudes, measurements that are unlikely with respect to the climatology can be considered biased and

AMTD
4, 7337–7403, 2011

therefore of poor quality. This data quality check could be used to reject measurements that fall outside of reasonable limits, but given the many years of biased Raman lidar data that already exist and which could potentially be made useful for atmospheric studies in the upper troposphere, it makes more sense to correct the data. Correcting the data is also consistent with the recommendations of the international metrology community (JCGM/GUM, 2008) which has stated, "It is assumed that the result of a measurement has been corrected for all recognized significant systematic effects and that every effort has been made to identify such effects". For the situation where the observed bias manifests itself as an essentially constant offset in ppmv space, such as the offset shown above 14 km for the ALVICE system in Fig. 2, the correction developed here for signal dependent bias may be implemented. The uncertainty of the correction amounted to approximately 4 % of the measured value at 200 hPa for the case of the ALVICE lidar data studied here. This increase in uncertainty is small considering the tolerance of water vapor measurements to relatively high uncertainties (Whiteman et al., 2011b) for the purposes of upper tropospheric trend detection. Given that water vapor increases are expected to be larger in the upper troposphere than lower stratosphere in the future, it is possible that future corrections using this same technique will contribute a similarly small or smaller uncertainty to measurements in the upper troposphere. If biases are believed to be due to fluorescence of airborne particles (Pan et al., 1999; Pinnick et al., 2004; Immler et al., 2005), the data quality control aspect of the technique described here may be used to reject the data.

Raman water vapor lidar has proven to be an extremely valuable research tool for many scientific applications and it is expected that it can be so within the context of the NDACC network as well. However, experience has taught that measurements of water vapor with Raman lidar, particularly in the dry upper troposphere and lower stratosphere, present extreme challenges that must be addressed with great care. It is for this reason that we suggest that protocols be developed within the NDACC Raman water vapor lidar effort with the focus being on delivering quality controlled data products with sufficient accuracy for specific scientific applications.

AMTD
4, 7337–7403, 2011

Appendix A

RS92 RH accuracy and corrections

The accuracy of RS92 relative humidity (RH) measurements during MOHAVE-2009 is evaluated by comparing to two reference sensors of known accuracy: dual soundings with frostpoint hygrometers, and comparisons before launch with the Temperature-Humidity-Pressure reference system (THPref). The THPref is a surface reference system that provides NIST traceable measurements of temperature, relative humidity and pressure and contains a ventilated chamber for characterizing radiosonde accuracy prior to launch. The uncertainty of the "best estimate" (averaged) THPref measurements are ±0.1°C, ±0.5 % RH, ±0.08 hPa, respectively. The measurements acquired during the time that radiosondes were inserted into the ventilated chamber were used to study radiosonde calibration errors and corrections. The THPref (Fig. 10, left side) consists of six calibrated Temperature (T) and Relative Humidity (RH) probes in a fan-ventilated chamber within a naturally-ventilated instrument shelter, into which radiosondes are placed for comparative measurements prior to launch. The purpose of using multiple probes is both to reduce the random error of the measurement and to provide redundancy. The Reference system that travels with the ALVICE trailer was developed by Milo Scientific of Lafayette, CO and is based on the original system developed by the DOE/ARM program and described in Miloshevich et al. (2009). We have augmented the instrument, which is now referred to as THPref, by addition of a precision barometer outside of the ventilated chamber the readings from which are coupled into the instrument data stream. During MOHAVE-2009 campaign, however, the P data were provided by the pressure sensor used with the SuomiNet GPS system. A comparison of the THPref RH measurements and those of a dual sensor RS92 radiosonde during the time of insertion of the sonde in the ventilated chamber is shown on the right side of Fig. 10. Analysis of the THPref and RS92 raw pre-launch data gives the calibration bias of RS92 T and RH measurements relative to THPref under surface conditions.

AMTD
4, 7337–7403, 2011

The THPref comparisons describe the RS92 accuracy under ambient conditions at the surface, and the comparisons with FPs and redundant RS92 sondes launched on the same balloons launched during MOHAVE-2009 (Hurst et al., 2011b) are used to characterize the RS92 accuracy in flight. During MOHAVE-2009 two versions of frostpoint hygrometers were launched, the CFH by TMF personnel and the NOAA FPH by NOAA personnel (Hurst et al., 2011b). On all of these launches an RS92 was flown as part of the payload. In the analysis of the RS92 RH measurement accuracy, the two versions of frostpoint hygrometer were used equivalently. The frostpoint hygrometer data are henceforth referred to generically as FP data.

Corrections for several known sources of measurement error were applied to the RS92 RH data following a modified approach to that described in Miloshevich et al. (2009). Recent work (Kottayil et al., 2011) has demonstrated that generation of the empirical correction as a function of temperature, as opposed to pressure as was done previously, is more consistent with the calibration of the radiosonde sensors and improves performance in the tropical UTLS. It is this more recent version of the correction that is used here. A component of the correction is for sensor time-lag error and helps to recover vertical structure in the profile that is "smoothed" by slow sensor response at temperatures below about −45 °C (Miloshevich et al., 2004). A correction is also applied for mean calibration bias, which is a moist bias in the lower troposphere and a dry bias at higher levels. A correction was also applied to the few daytime soundings for solar radiation dry bias caused by solar heating of the RH sensor. The bias corrections were derived to remove the mean bias of 2006–2007 vintage RS92 measurements relative to 3 reference sensors: frostpoint hygrometer above the 700 mb level, a THref system at the surface, and microwave radiometer (MWR) precipitable water measurements that represent mainly the lower troposphere. The RS92 RH accuracy and the correction for mean calibration bias are evaluated here by similar comparisons of the nighttime MOHAVE-2009 RS92 measurements to the FP and THPref reference sensors.

AMTD
4, 7337–7403, 2011

For 41 RS92-THPref comparisons during MOHAVE-2009, the mean and standard deviation of the RS92 RH and T biases were $+1.6 \pm 0.4$ % RH and $+0.09 \pm 0.16$°C. In terms of water vapor mixing ratio (Fig. 11, left), the RS92 mean moist bias relative to THPref was $+6.2 \pm 3.4$ %, and it varies with RH from about +12 % at 15 % RH to <3 % above 50 % RH. The ±0.5 % RH uncertainty of the THPref measurements is half the magnitude of the curved dashed lines. The correction for mean calibration bias (Fig. 11, right) mostly removes the RS92 mean bias and its RH-dependence, but it appears to overcorrect by about 1 % for conditions above 30 % RH. Most likely the over-correction reflects periodic re-calibration of the Vaisala factory references and possibly changes to the Vaisala calibration function since the 2006–2007 timeframe. This illustrates an important point that the mean calibration bias is expected to change with time and therefore a correction becomes out-of-date, unlike corrections for time-lag and solar radiation errors that only change with physical changes to the sensor or manufacturing process, or if Vaisala institutes their own corrections, which they have done for time-lag and solar radiation errors beginning with Digicora softare version 3.64 released in December 2010.

For the 24 nighttime FP and RS92 dual soundings conducted during MOHAVE-2009, the RS92 had a moist mean bias relative to FP of about 5 % in the lower troposphere, and at higher levels it had a dry mean bias that increased with height to a maximum of 40 % in the tropopause region (Fig. 12, left). The calibration correction (Fig. 12, right) over-corrects in the lower troposphere by about the same magnitude as the measured mean bias, so it neither increases nor decreases the RS92 accuracy. At higher levels the calibration correction under-corrects by about 10 % up to 12 km altitude, increasing to a maximum of 25 % in the tropopause region. Time-lag error is also a factor in the UTLS when humidity gradients are steep, most notably around 19 km where the RH consistently decreases to low stratospheric values due to the increase in temperatures coupled with a nearly constant water vapor mixing ratio. Again it is thought that the calibration correction is less effective for 2009 radiosondes than for 2006–2007 radiosondes due to expected changes in the mean calibration bias with time.

AMTD
4, 7337–7403, 2011

Altitude profiles of the RS92 accuracy relative to FP can be misleading because they describe all RH conditions combined, whereas the RS92 calibration bias varies with RH. Extremely dry conditions were frequently encountered during MOHAVE-2009, when a small bias of 0.5 % RH is relatively large (e.g. 50 % bias at 1 % RH). Figure 13 shows the same data as Fig. 12, but the RS92 bias relative to FP is shown in 4 RH intervals. The over-correction in the lower troposphere (rightmost dots) applies to all RH conditions, but the under-correction at lower pressures is only seen for conditions of RH < 20 % and especially RH < 10 %.

The uncertainty in corrected RS92 RH measurements can be estimated from the bias uncertainty of ±(4 % + 0.5 % RH) given in Miloshevich et al. (2009), which is based on the size of the dataset used to derive the correction and the uncertainty in FP measurements. The constant 0.5 % RH component of uncertainty reflects the accuracy of the 0 % RH calibration and uncertainty in the Vaisala ground-check at 0 % RH. The random component of uncertainty (the 2-sigma sonde-to-sonde "production variability") was estimated from dual RS92 soundings to be ±3 % (for RH > 10 %) or ±6 % (for RH ≤ 10 %). The estimated total uncertainty for corrected RS92 measurements is the RMS sum of the bias and random components, or ±(5 % + 0.5 % RH) for RH > 10 % and ±(7 % + 0.5 % RH) for RH ≤ 10 %, which corresponds to an uncertainty of ±6 % at 50 % RH, ± 10 % at 10 % RH, and ±24 % at 3 % RH. The comparison to FP in Fig. 13 is consistent with this uncertainty estimate, but still there is evidence that the mean calibration bias for 2009 radiosondes has changed relative to the 2005–2008 radiosondes described by the above uncertainty estimate, due to expected changes in the RS92 calibration with time, and indicating that the uncertainty estimate for 2005–2008 radiosondes is conservative.

Acknowledgements. The authors wish to acknowledge the NASA Atmospheric Composition Program, managed by Ken Jucks, for support of these efforts. The mention of a particular vendor does not constitute an endorsement by NASA.

AMTD
4, 7337–7403, 2011

References

Ackerman, T. and Stokes, G.: The Atmospheric Radiation Measurement program, Phys. Today, 56, 38–45, 2003. 7361

Behrendt, A. and Reichardt, J.: Atmospheric temperature profiling in the presence of clouds with a pure rotational Raman lidar by use of an interference-filter-based polychromator, Appl. Optics, 39(9), 1372–1378, 2000. 7342

Behrendt, A., Wulfmeyer, V., Di Girolamo, P., Kiemle, C., Bauer, H.-S., Schaberl, T., Summa, D., Whiteman, D. N., Demoz, B. B., Browell, E. V., Ismail, S., Ferrare, R., Kooi, S., Ehret, G., Wang, J.: "Intercomparison of water vapor data measured with lidar during IHOP_2002, Part 1: Airborne to ground-based lidar systems and comparisons with chilled-mirror hygrometer radiosondes.", J. Atmos. Oceanic Technol., 24(1), 3–21, doi:10.1175/JTECH1924.1, 2007. 7365

Boens, N., Qin, W., Basarić, N., Hofkens, J., Ameloot, M., Pouget, J., Lefèvre, J. P., Valeur, B., Gratton, E., vandeVen, M., Silva, N. D. Jr., Engelborghs, Y., Willaert, K., Sillen, A., Rumbles, G., Phillips, D., Visser, A. J., van Hoek, A., Lakowicz, J. R., Malak, H., Gryczynski, I., Szabo, A. G., Krajcarski, D. T., Tamai, N., and Miura, A.: Fluorescence lifetime standards for time and frequency domain fluorescence spectroscopy, Anal. Chem., Mar 1, 79, 2137–2149, Epub 2007 Feb 1, 2007. 7353

Boers, R. and Meijgaard, E.: What are the demands on an observational program to detect trends in upper tropospheric water vapor anticipated in the 21st century,GRL, in press, 2009. 7340, 7368, 7372

Brydegaard, M., Guan, Z., Wellenreuther, M., and Svanberg, S.: Insect monitoring with fluorescence lidar techniques: feasibility study, Appl. Optics, 48(30), 20 October 5668–5677, 2009. 7345

Di Girolamo, P., Marchese, R., Whiteman, D. N., and Demoz, B. B.: Rotational Raman lidar measurements of atmospheric temperature in the UV, Geophys. Res. Lett., 31, L01106, doi:10.1029/2003GL018342, 2004. 7342

Dionisi, D., Congeduti, F., Liberti, G. L., and Cardilloc, F.: Calibration of a Multichannel Water Vapor Raman Lidar through Noncollocated Operational Soundings: Optimization and Characterization of Accuracy and Variability, J. Atmos. Ocean. Tech., 27, 108–121, doi:10.1175/2009JTECHA1327, 2009. 7348

Dvorak, M. A., Oswald, G. A., Van Benthem, M. H., and Gillispie, G. D.: On-the-Fly Fluo-

AMTD
4, 7337–7403, 2011

rescence Lifetime Determination with Total Emission Detection in HPLC, Anal. Chem., 69, 3458–3464, 1997. 7353
Ferrare, R. A., Browell, E. V., Ismail, S., Kooi, S. A., Brasseur, L. H., Brackett, V. G., Clayton, M. B., Barrick, J. D. W., Diskin, G. S., Goldsmith, J. E. M., Lesht, B. M., Podolske, J. R., Sachse, G. W., Schmidlin, F. J., Turner, D. D., Whiteman, D. N., Tobin, D., Miloshevich, L. M., Revercomb, H. E., Demoz, B. B., and Di Girolamo, P.: Characterization of Upper-Troposphere Water Vapor Measurements during AFWEX Using LASE, J. Atmos. Ocean. Tech., 21, 1790–1808, 2004. 7346, 7348
Free, M., Durre, I., Aguilar, E., Seidel, D., Peterson, T. C., Eskridge, R. E., Luers, J. K., Parker, D., Gordon, M., Lanzante, J., Klein, S., Christy, J., Schroeder, S., Soden, B., McMillin, L. M., and Weatherhead, E.: Creating Climate Reference Datasets - CARDS Workshop on Adjusting Radiosonde Temperature Data for Climate Monitoring, Bull. Amer. Meteor., Soc., 891–899, June, 2002. 7374, 7377
GCOS Reference Upper-Air Network (GRUAN): Justification, requirements, siting and instrumentation options – April GCOS-112, 2007.
Gelbwachs, J. and Birnbaum, M.: Fluorescence of Atmospheric Aerosols and Lidar Implications, Appl. Opt., 12(10), October 1973. 7348, 7377
GRUAN Implementation Plan 2009–2013, GCOS-134, July, 2009.
Harms, J., Lahmann, W., and Weitkamp, C.: Geometrical Compression of Lidar Return Signals: Appl. Opt., 17(7), 1131–1135, 1978. 7365
Held, I. M. and Soden, B. J.: "Robust Responses of the Hydrological Cycle to Global Warming", J. Climate, 19, 5686–5699, 2006. 7340, 7368
Hurst, D. F., Oltmans, S. J., Vömel, H., Rosenlof, K. H., Davis, S. M., Ray, E. A., Hall, E. G., and Jordan, A. F.: Stratospheric water vapor trends over Boulder, Colorado: Analysis of the 30 year Boulder record, J. Geophys. Res., 116, D02306, doi:10.1029/2010JD015065, 2011a. 7368
Hurst, D. F., Hall, E. G., Jordan, A. F., Miloshevich, L. M., Whiteman, D. N., Leblanc, T., Walsh, D., Vömel, H., and Oltmans, S. J.: Comparisons of temperature, pressure and humidity measurements by balloon-borne radiosondes and frost point hygrometers during MOHAVE 2009, Atmos. Meas. Tech. Discuss., 4, 4357–4401, doi:10.5194/amtd-4-4357-2011, 2011b. 7343, 7369, 7380
Immler, F. J., Engelbart, D., and Schrems, O.: Fluorescence from atmospheric aerosol detected by a lidar indicates biogenic particles in the lowermost stratosphere, Atmos. Chem. Phys., 5,

AMTD
4, 7337–7403, 2011

345–355, doi:10.5194/acp-5-345-2005, 2005. 7347, 7377, 7378
Immler, F. J., Dykema, J., Gardiner, T., Whiteman, D. N., Thorne, P. W., and Vömel, H.: Reference Quality Upper-Air Measurements: guidance for developing GRUAN data products, Atmos. Meas. Tech., 3, 1217–1231, doi:10.5194/amt-3-1217-2010, 2010.
Kotayil, A., Buehler, S. A., John, V. O., Miloshevich, L. M., Milz, M., and Holl, G.: On the importance of radiosonde corrections for a better agreement between satellite and radiosonde measurements, J. Atmos. Ocean. Tech., accepted, 2011. 7380
Lambert, A., Read, W. G., Livesey, N. J., Santee, M. L., Manney, G. L., Froidevaux,L., Wu, D. L., Schwartz, M. J., Pumphrey,M., Jimenez, C., Nedoluha, G. E., Cofield, R. E., Cuddy, D. T., Daffer, W. F., Drouin, B. J., Fuller, R. A., Jarnot, R. F., Knosp, B. W., Pickett, H. M., Perun, V. S., Snyder, W. V., Stek, P. C., Thurstans, R. P., Wagner, P. A., Waters, J. W., Jucks, K. W.,Toon, G. C., Stachnik, R. A., Bernath, P. F., Boone, C. D., Walker, K. A., Urban, J., Murtagh, D., Elkins, J. W., and Atlas, E.: Validation of the Aura Microwave Limb Sounder middle atmosphere water vapor and nitrous oxide measurements, J. Geophys. Res., 112, D24S36, doi:10.1029/2007JD008724, 2007. 7369
Leblanc, T. and McDermid, I. S.: Accuracy of Raman lidar water vapor calibration and its applicability to long-term measurements, Appl. Opt., 47, 30, 5592–5603, 2008. 7358
Leblanc, T. and McDermid, I. S.: Reply to "Comments on Accuracy of Raman lidar watervapor calibration and its applicability to long-term measurements by Whiteman et al.", 50, 2177–2178, 2011. 7358
Leblanc, T., McDermid, I. S., and Aspey, R. A.: First-Year Operation of a New Water Vapor Raman Lidar at the JPL Table Mountain Facility, California, J. Atmos. Ocean. Tech., 25, 1454–1462, 2007. 7366
Leblanc, T., McDermid, I. S., and Walsh, T. D.: Ground-based water vapor Raman lidar measurements up to the upper troposphere and lower stratosphere — Part 2: Data analysis and calibration for long-term monitoring, Atmos. Meas. Tech. Discuss., 4, 5111–5145, doi:10.5194/amtd-4-5111-2011, 2011a. 7367
Leblanc, T., Walsh, T. D., McDermid, I. S., Toon, G. C., Blavier, J.-F., Haines, B., Read, W. G., Herman, B., Fetzer, E., Sander, S., Pongetti, T., Whiteman, D. N., McGee, T. G., Twigg, L., Sumnicht, G., Venable, D., Calhoun, M., Dirisu, A., Hurst, D., Jordan, A., Hall, E., Miloshevich, L., Vömel, H., Straub, C., Kampfer, N., Nedoluha, G. E., Gomez, R. M., Holub, K., Gutman, S., Braun, J., Vanhove, T., Stiller, G., and Hauchecorne, A.: Measurements of Humidity in the Atmosphere and Validation Experiments (MOHAVE)-2009: overview of cam-

AMTD
4, 7337–7403, 2011

paign operations and results, Atmos. Meas.Tech. Discuss., 4, 3277–3336, doi:10.5194/amtd-4-3277-2011, 2011b. 7340, 7364, 7373

Livesey, N. J., Read, W. G., Froidevaux, L., Lambert, A., Manney, G. L., Pumphrey, H. C., Santee, M. L., Schwartz, M. J., Wang, S., Cofield, R. E., Cuddy, D. T., Fuller, R. A., Jarnot, R. F., Jiang, J. H., Knosp, B. W., Stek, P. C., Wagner, P. A., and Wu, D. L.: Version 3.3 level 2 data quality and description document., Jet Propulsion Laboratory/California Institute of Technology, JPL, 33509, 156 pp., available at: http://mls.jpl.nasa.gov/data/v3-3_data_quality_document.pdf, 2011. 7370

Mastenbrook, H. J. and Dinger, J. E. : Distribution of water vapor in the stratosphere, J. Geophys. Res., 66, 1437–1444, 1961.

McDermid, I. S., Leblanc, T., and Walsh, T. D.: Ground-based water vapor Raman lidar measurements up to the upper troposphere and lower stratosphere — Part 1: Instrument development, optimization, and validation, Atmos. Meas. Tech. Discuss., 4, 5079–5109, doi:10.5194/amtd-4-5079-2011, 2011.

Miloshevich, L. M., Paukkunen, A., Vömel, H., and Oltmans, S. J.: Development and validation of a time-lag correction for Vaisala radiosonde humidity measurements, J. Atmos. Oceanic Technol., 21, 1305–1327, 2004. 7380

Miloshevich, L. M., Voemel, H., Whiteman, D., Lesht, B., Schmidlin, F. J., and Russo, F.: Absolute accuracy of water vapor measurements from six operational radiosonde types launched during AWEX-G and implications for AIRS validation, J. Geophys. Res., 111, doi:10.1029/2005JD006083, 2006. 7347

Miloshevich, L. M., Vömel, H., Whiteman, D. N., and Leblanc, T.: Accuracy Assessment and Correction of Vaisala RS92 radiosonde water vapor measurements, J. Geophys. Res., 114, D11305, doi:10.1029/2008JD011565, 2009. 7358, 7360, 7375, 7379, 7380, 7382

Oman, L., Waugh, D., Pawson, S., Stolarski, R., and Nielsen, J.: Understanding the Changes of Stratospheric Water Vapor in Coupled Chemistry–Climate Model Simulations, J. Atmos. Sci., 65, 3278–3291, 2008. 7368, 7374

Pan, Y.-Le, Holler, S., Chang, R. K., Hill, S. C., Pinnick, R. G., Niles, S., and Bottiger, J. R.: Single-shot fluorescence spectra of individual micrometer-sized bioaerosols illuminated by a 351- or a 266-nm ultraviolet laser, Opt. Lettr., 24(2), January 15, 1999. 7348, 7377, 7378

Pinnick, R. G., Hill, S. C., Pan, Y.-Le, and Chang, R. K.: Fluorescence spectra of atmospheric aerosol at Adelphi, Maryland, USA: measurement and classification of single particles containing organic carbon, Atmos. Env., 38, 1657–1672, 2004. 7348, 7377, 7378

AMTD
4, 7337–7403, 2011

Piironen, P.: Data System in "A High Spectral Resolution Lidar Based on an Iodine Absorption Filter", Ph.D. Thesis, University of Joensuu, Department of Physics, Finland, 1994. 7355
Report of the GCOS Reference Upper-Air Network Implementation Meeting, Lindenberg, Germany, GCOS-121, 26–28 February, 2008.
Report of the First GCOS Reference Upper Air Network Implementation and Coordination Meeting (GRUAN ICM-1), Norman, Oklahoma, USA, GCOS-131, 2–4 March, 2009.
Report of the Second GCOS Reference Upper Air Network Implementation and Coordination Meeting (GRUAN ICM-2), Payerne, Switzerland,GCOS-140, 2–4 March, 2010.
Sakai, T., Nagai, T., Nakazato, M., Matsumura, T., Orikasa, N., and Shoji, Y.: Comparisons of Raman lidar measurements of tropospheric water vapor profiles with radiosondes, hygrometers on meteorological observation tower, and GPS at Tsukuba, Japan, J. Atmos, Ocean. Techn., 24, 1407–1423, 2007. 7348
Saito, Y., Kobayashi, K., and Kobayashi, F.: Laser-induced Fluorescence Spectrum (LIFS) Lidar for Remote Detection of Biological Substances Surrounding the ""Livingsphere", The 8th International Symposium on Advanced Environmental Monitoring, Hokaido, Japan, 2010. 7347
Seidel, D. J., Berger, F., Diamond, H., Dykema, J., Goodrich, D., Immler, F., Murray, W., Peterson, T., Sisterson, D., Sommer, M., Thorne, P., Vomel, H., Wang, J.: Reference Upper-Air Observations for Climate: Rationale, Progress, and Plans. Bulletin of the American Meteorological Society, March 2009.
Seidel, D. J., Angell, J. K., Christy, J., Free, M., Klein, S. A., Lanzante, J. R., Mears, C., Parker, D., Schable, M., Spenscer, R., Stern, A., Thorne, P., and Wentz, F.: Uncertainty in signals of large-scale climate variations in radiosonde and satellite upper-air temperature datasets, J. Clim., 17, 2225–2240, 2004. 7374
Sherlock, V., A. Garnier, A. Hauchecorne, P. Keckhut, Implementation and validation of a Raman lidar measurement of middle and upper tropospheric water vapor, App. Opt., 38, 27, 5838–5850, 1999. 7346
Soden, B. J., Jackson, D. L., Ramaswamy, V., Schwarzkopf, M. D., and Huang, X.: The radiative signature of upper tropospheric moistening, Science, 310, 5749, 841–844, 2005. 7340, 7368, 7372
Solomon, S., Rosenlof, K., Portmann, R., Daniel, J., Davis, S., Sanford, T., Plattner, G. -K.: Contributions of Stratospheric Water Vapor to Decadal Changes in the Rate of Global Warming, Science, 327, 1219–1223, 2010. 7372

AMTD
4, 7337–7403, 2011

Stiller, G. P., Kiefer, M., Eckert, E., von Clarmann, T., Kellmann, S., García-Comas, M., Funke, B., Leblanc, T., Fetzer, E., Froidevaux, L., Gomez, M., Hall, E., Hurst, D., Jordan, A., Kämpfer, N., Lambert, A., McDermid, I. S., McGee, T., Miloshevich, L., Nedoluha, G., Read, W., Schneider, M., Schwartz, M., Straub, C., Toon, G., Twigg, L. W., Walker, K., and Whiteman, D. N.: Validation of MIPAS IMK/IAA temperature, water vapor, and ozone profiles with MOHAVE-2009 campaign measurements, Atmos. Meas. Tech. Discuss., 4, 4403–4472, doi:10.5194/amtd-4-4403-2011, 2011. 7342, 7367

Tiao, G. C., Reinsel, G. C., Xu, D., Pedrick, J. H., Zhu, Z., Miller, A. J., DeLuisi, J. J., and Wuebbles, D. J.: Effects of Autocorrelation and Temporal Sampling Schemes on Estimates of Trend and Spatial Correlation, J. Geophys. Res., 95(D12), 20507–20517, November 20, 1990.

Tobin, D. C., Revercomb, H. E., Knuteson, R. O., Lesht, B. M., Strow, L. L., Hannon, S. E., Feltz, W. F., Moy, L. A., Fetzer, E. J., and Cress, T. S.: Atmospheric Radiation Measurement site atmospheric state best estimates for Atmospheric Infrared Sounder temperature and water vapor retrieval validation, J. Geophys. Res., 111, D09S14, doi:10.1029/2005JD006103, 2006 7361

Turner, D. D., Ferrare, R. A., Heilman Breasseur, L. A., Feltz, W. F., and Tooman, T. P.: Automated Retrievals of Water Vapor and Aerosol Profiles from an Operational Raman Lidar, JTECH, 19, 37–50, 2000. 7348, 7365

VDI4210, Blatt1, Remote Sensing Atmospheric Measurements with LIDAR – Measuring gaseous air pollution with DAS Lidar, Verein Deutscher Ingenieure, ICS 13.040.20; 17.180.01, 1999. 7371

Venable, D. D., Whiteman, D. N., Calhoun, M. N., Dirisu, A. O., Connell, R. M., and Landulfo, E.: A Lamp Mapping Technique for Independent Determination of the Water Vapor Mixing Ratio Calibration Factor for a Raman Lidar System, Appl. Opt., 50, 4622—4632, 2011. 7359

Vömel, H., David, D. E., and Smith, K.: Accuracy of tropospheric and stratospheric water vapor measurements by the cryogenic frost point hygrometer: Instrumental details and observations, J. Geophys. Res., 112, D08305, doi:10.1029/2006JD007224, 2007a. 7343

Vömel, H., Barnes, J. E., Forno, R. N., Fujiwara, M., Hasebe, F., Iwasaki, S., Kivi, R., Komala, N., Kyro, E., Leblanc, T., Morel, B., Ogino, S.-Y., Read, W. G., Ryan, S. C., Saraspriya, S., Selkirk, H., Shiotani, M., Valverde Canossa, J., and Whiteman, D. N.: Validation of Aura Microwave Limb Sounder water vapor by balloonborne Cryogenic Frost point Hygrometer measurements, J. Geophys. Res., 112, D24S37, doi:10.1029/2007JD00869, 2007b. 7360,

AMTD
4, 7337–7403, 2011

7369
Ware, R. H., Fulker, D. W., Stein, S. A., Anderson, D. N., Avery, S. K., Clark, R. D., Droegemeier, K. K., Kuettner, J. P., Minster, J. B., Sorooshian, S.: SuomiNet: A Real-Time National GPS Network for Atmospheric Research and Education, 81(4), 677–694, 2000. 7341, 7365
Weatherhead, E. C., Reinsel, G. C., Tiao, G. C., Meng, X.-Li, Choi, D., Cheang, W-K., Keller, T., DeLuisi, J., Wuebbles, D. J., Kerr, J. B., Miller, A. J., Oltmans, S. J., and Frederick, J. E.: Factors affecting the detection of trends: Statistical considerations and applications to environmental data, J. Geophys. Res., 103(D14), 17149–17161, 27 July, 1998.
Weatherhead, E. C., Stevermer, A. J., and Schwartz, B. E.: Detecting environmental changes and trends, Phys. Chem. Earth, 27, 399–403, 2002.
Whiteman, D. N.: Examination of the traditional Raman lidar technique. I. Evaluating the temperature-dependent lidar equations, Appl. Optics, 42(15), 2571–2592, 2003a. 7350, 7351
Whiteman, D. N.: Examination of the traditional Raman lidar technique. II. Evaluating the ratios for water vapor and aerosols, Appl. Optics, 42(15), 2593–2608, 2003b. 7350
Whiteman, D. N., Demoz, B., Di Girolamo, P., Comer, J., Veselovskii, I., Evans, K., Wang, Z., Cadirola, M., Rush, K., Sabatino, D., Schwemmer, G., Gentry, B., Melfi, S. H., Mielke, B., Venable, D., Van Hove, T., Browell, E., Ferrare, R., Ismail, S., and Wang, J.: Raman Water Vapor Lidar Measurements During the International H_2O Project. I. Instrumentation and Analysis Techniques, J. Atmos. Oceanic Technol., 23, 157–169, 2006a. 7365, 7366
Whiteman, D. N., Demoz, B., Di Girolamo, P. , Comer, J., Veselovskii, I., Evans, K., Wang, Z., Cadirola, M., Rush, K., Sabatino, D., Schwemmer, G., Gentry, B., Melfi, S. H., Mielke, B., Venable, D., Van Hove, T., Browell, E., Ferrare, R., Ismail, S., and Wang, J.: Raman Water Vapor Lidar Measurements During the International H_2O Project. II. Instrument Comparisons and Case Studies, J. Atmos. Oceanic Technol., 23, 170–183, 2006b. 7365
Whiteman, D. N., Russo, Miloshevich, F. L., Demoz, B., Wang, Z., Veselovskii, I., Voemel, H., Hannon, S., Lesht, B., Schmidlin, F., Gambacorta, A., and Barnet, C.: Analysis of Raman lidar and radiosonde measurements from the AWEX-G field campaign and its relation to Aqua validation, J. Geophys. Res., 111, D09S09, doi:10.1029/2005JD006429, 2006. 7346, 7347, 7361, 7365
Whiteman, D. N., Veselovskii, I., Cadirola, M., Rush, K., Comer, J., Potter, J., and Tola, R.: Demonstration Measurements of Water Vapor, Cirrus Clouds, and Carbon Dioxide Using a High-Performance Raman Lidar, J. Atmos. Ocean. Tech., 24(8), 1377–1388, 2007. 7341

AMTD
4, 7337–7403, 2011

Whiteman, D. N., Rush, K., Rabenhorst, S., Welch, W., Cadirola, M., McIntire, G., Russo, F., Adam, M., Venable, D., Connell, R., Veselovskii, I., Forno, R., Mielke, B., Stein, B., Leblanc, T., McDermid, S., and Vömel, H.: Airborne and Ground-based measurements using a High-Performance Raman Lidar, 27, 1781–1801, doi:10.1175/2010JTECHA1391, 2010. 7341, 7344, 7366, 7373

Whiteman, D. N., Venable, D. V., and Landulfo, E.: "Comments on: Accuracy of Raman lidar water vapor calibration and its applicability to long-term measurements", Appl. Opt., 1., 50(15), 2170–2176, 2011. 7358, 7359

Whiteman, D. N., Vermeesch, K. C., Oman, L. D., and Weatherhead, E. C.: The relative importance of random error and observation frequency in detecting trends in upper tropospheric water vapor, J. Geophys. Res., 116, D21118, doi:10.1029/2011JD016610, 2011.
7340, 7368, 7371, 7372, 7373, 7374, 7378

AMTD
4, 7337–7403, 2011

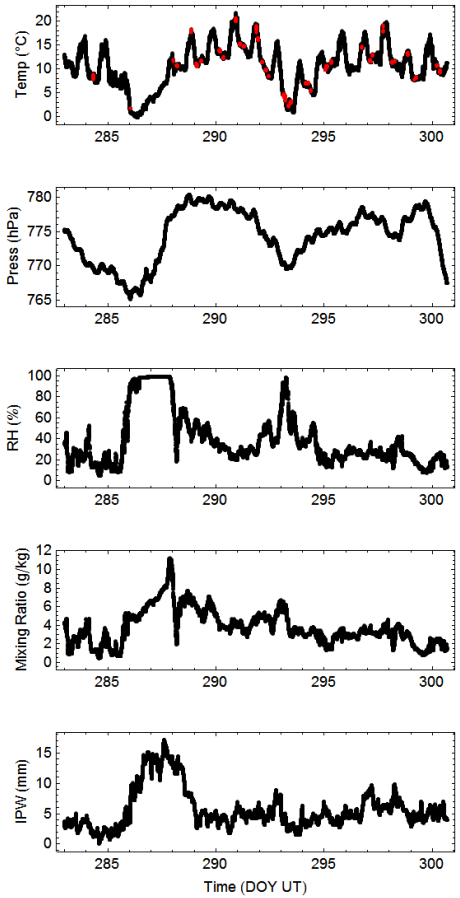

Fig. 1. Time series during MOHAVE-2009 of surface T, P, RH, mixing ratio and total column water from the THPRef and SuomiNet instruments that are part of the ALVICE instrumentation. The times when radiosondes were inserted into the ventilated chamber for comparative measurements are marked with red dots.

AMTD
4, 7337–7403, 2011

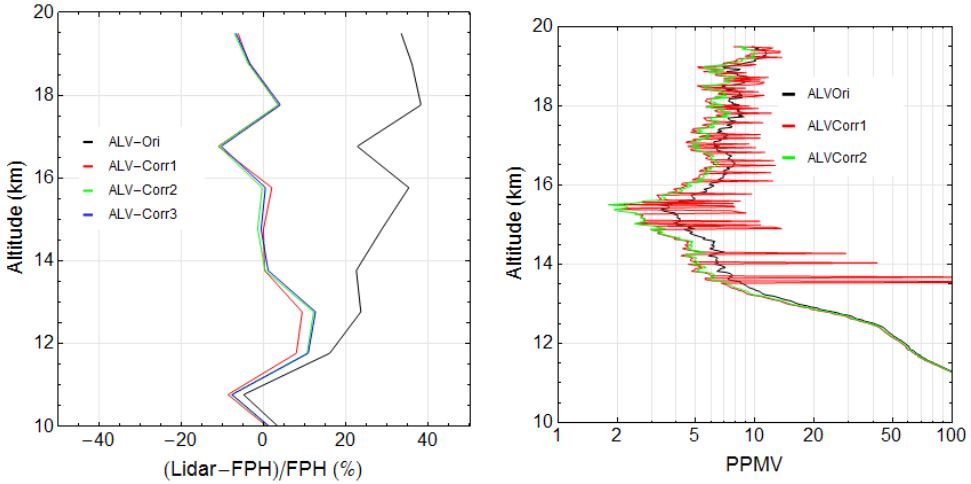

Fig. 2. (Left) Mean comparison of three correction equations using long duration measurements on 4 nights. (Right) Comparison of the the first two correction techniques using a single hour of lidar data.

AMTD
4, 7337–7403, 2011

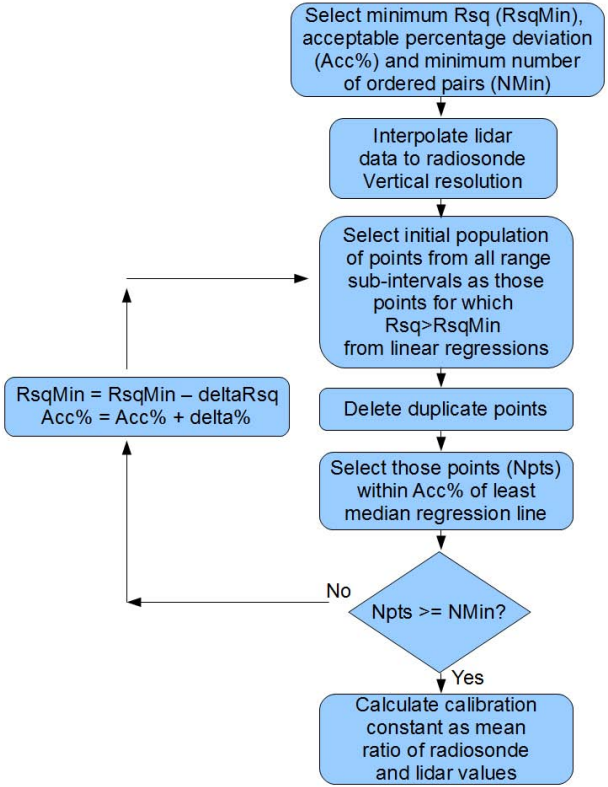

Fig. 3. Flow chart for the adaptive algorithm used to select geometrically similar portions of the lidar and radiosonde profiles for determining the lidar calibration constant. See text for more details.

AMTD
4, 7337–7403, 2011

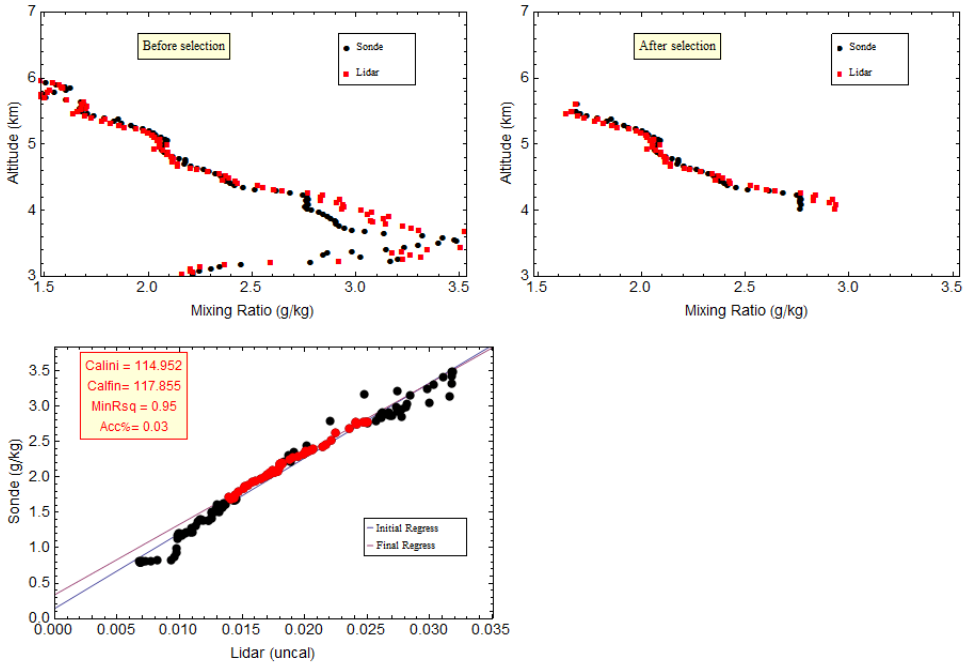

Fig. 4. Demonstration of the adaptive radiosonde calibration routine. In the upper left is shown both lidar (red) and radiosonde (black) profiles without data filtering. In the upper right is shown the sets of ordered pairs that are selected by the algorithm described in the text. On the bottom is shown the regression lines of the original set of lidar and sonde ordered pairs in black and the finally selected set in red.

AMTD
4, 7337–7403, 2011

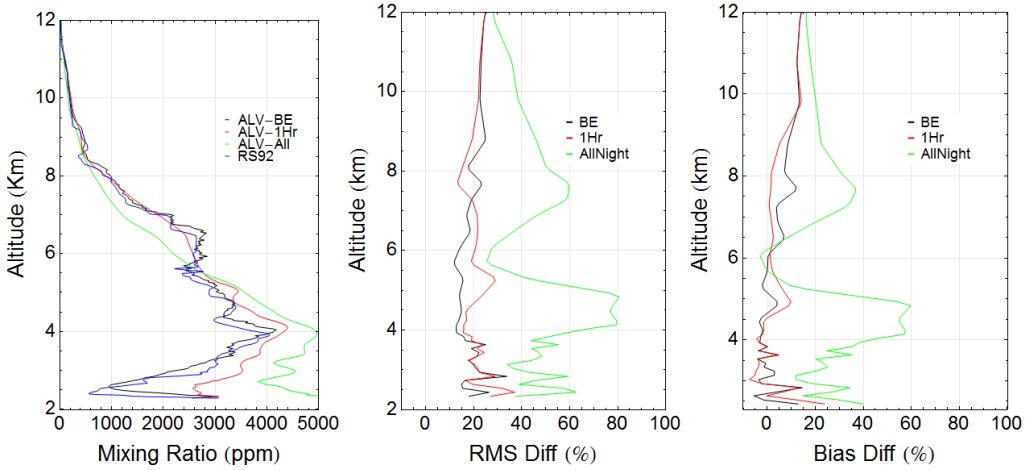

Fig. 5. (Left) Comparison of best esimate, 1-h sum and "all night" ALVICE profiles and the RS92 radiosonde launch on 25 October at 03:55 UT . Mean RMS (middle) and bias (right) of the different ALVICE data procucts with all available RS92 radiosonde launches.

AMTD
4, 7337–7403, 2011

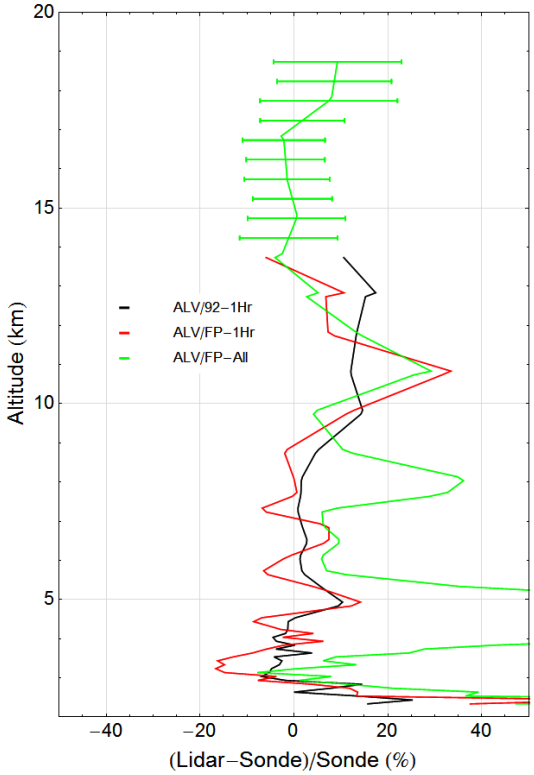

Fig. 6. Mean normalized differences of all available 1-h and all night sum ALVICE profiles with RS92 and FP. The standard deviation of the differences is plotted above 14 km for the FP all night lidar comparison. See text for detatils.

AMTD
4, 7337–7403, 2011

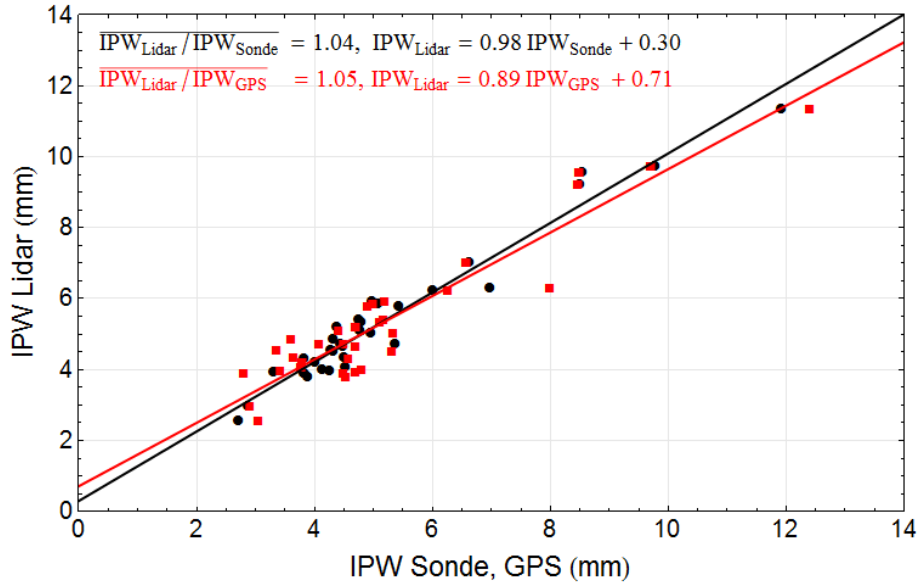

Fig. 7. Comparison of integrated precipitable water from the ALVICE lidar using the best estimate product and corrected RS92 (black) andSuomiNet GPS (red). The lidar results are 4–5 % drier than both the radiosonde and GPS.

AMTD
4, 7337–7403, 2011

Correction technique for raman water vapor lidar signal

D. N. Whiteman et al.

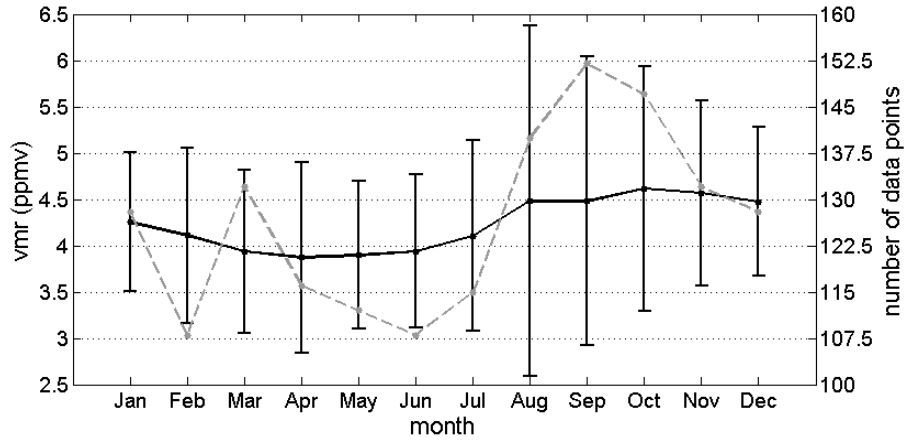

Fig. 8. Mean monthly water vapor mixing ratios (ppmv) measured by MLS over the altitude range of ~17–19.5 km. The average was computed using MLS v3.3 data from August, 2004 until February, 2011. The scale for the mixing ratio (solid black line) is on the left while the scale for the number of measurements used in each average (dashed grey line) is shown on the right. The error bars plotted are 2-sigma.

AMTD
4, 7337–7403, 2011

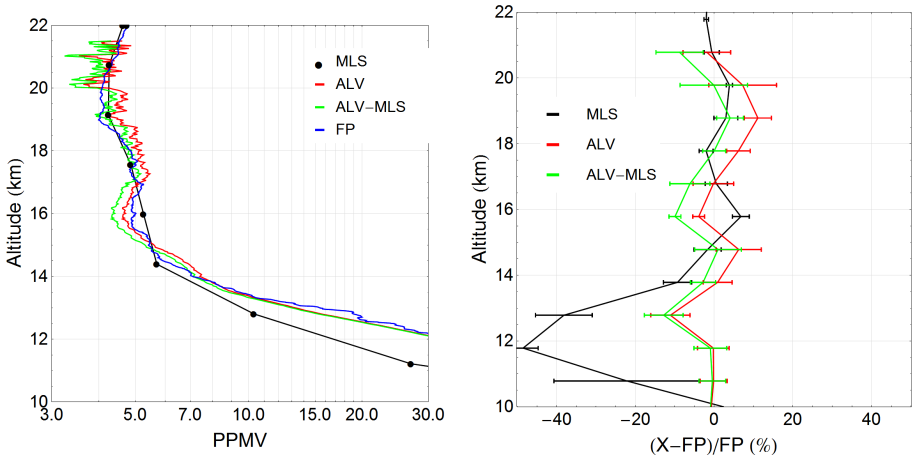

Fig. 9. (Left) Mean profiles of MLS, ALVICE (best estimate) and ALVICE (with correction based on MLS climatology) and FP for all data available during the MOHAVE campaign. (Right) Mean normalized differences in 1-km thick layers of MLS, ALV-best estimate, ALV-MLS corrected with frostpoint hygrometer using the same data as on the left.

AMTD
4, 7337–7403, 2011

Correction technique for raman water vapor lidar signal

D. N. Whiteman et al.

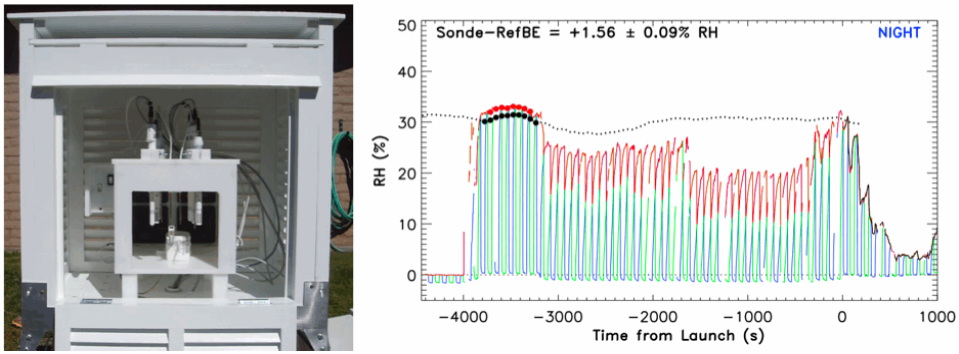

Fig. 10. On the left an RS92 is shown in the THPref, although normally the door is closed and faces north, and it is located away from buildings and other sources of heat or moisture. On the right is an example data comparison showing RH time series from the THPref (black dashed line) and RS92 (red prior to launch at $t = 0$, and black after launch). The large dots are 1-min averages during the comparison period when the RS92 is in the THPref, in this case indicating an RS92 mean bias relative to THPref of +1.6 % RH. Green and blue curves represent the individual RS92 RH sensors that are alternately heated while the other sensor measures, where the RS92 RH data (red curve) is given by the combined measurement portions from each sensor. Note that prior to launch, recovery from a heating cycle is incomplete when the RS92 is not being ventilated in the THPref.

AMTD
4, 7337–7403, 2011

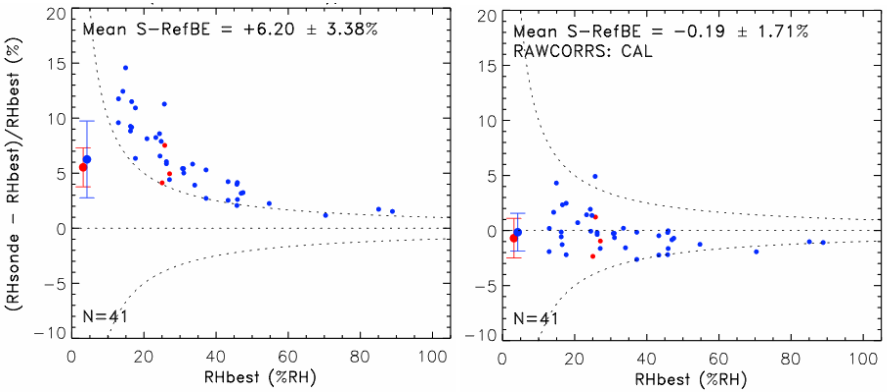

Fig. 11. Percentage difference between RS92 RH measurements and the mean of the 6 THPref probes, shown as a function of RH for the original RS92 measurements (left) and after applying the correction for mean calibration bias (right). Blue indicates nighttime measurements and red indicates daytime. The curved dashed lines represent a difference of ±1 % RH.

AMTD
4, 7337–7403, 2011

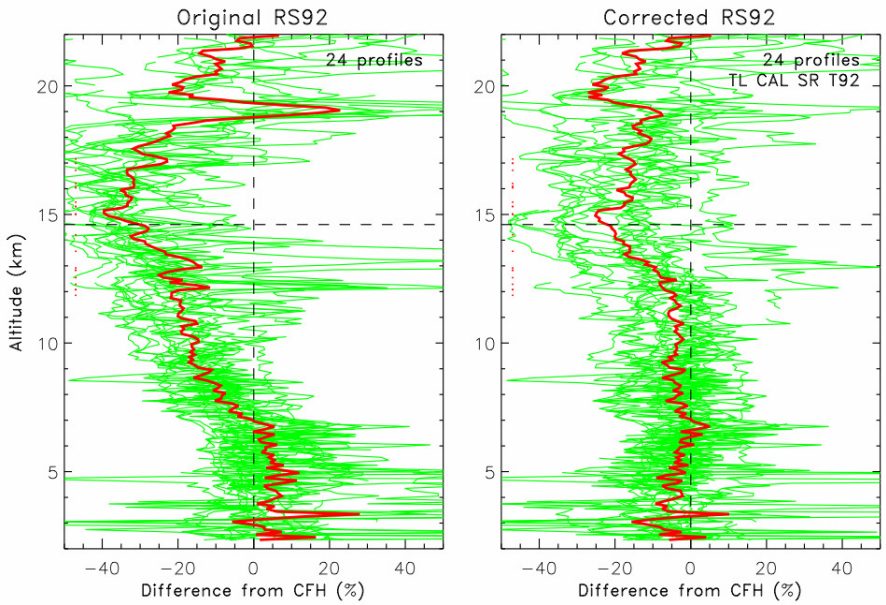

Fig. 12. Altitude profiles of the relative percentage difference between RS92 and frostpoint hygrometer (green) and the mean of all profiles (red) for the nighttime MOHAVE 2009 dual soundings, shown for the original RS92 measurements (left) and after applying the calibration and time-lag corrections (right). Dashed line is the mean tropopause height, and tiny red dots are the individual tropopause estimates.

AMTD
4, 7337–7403, 2011

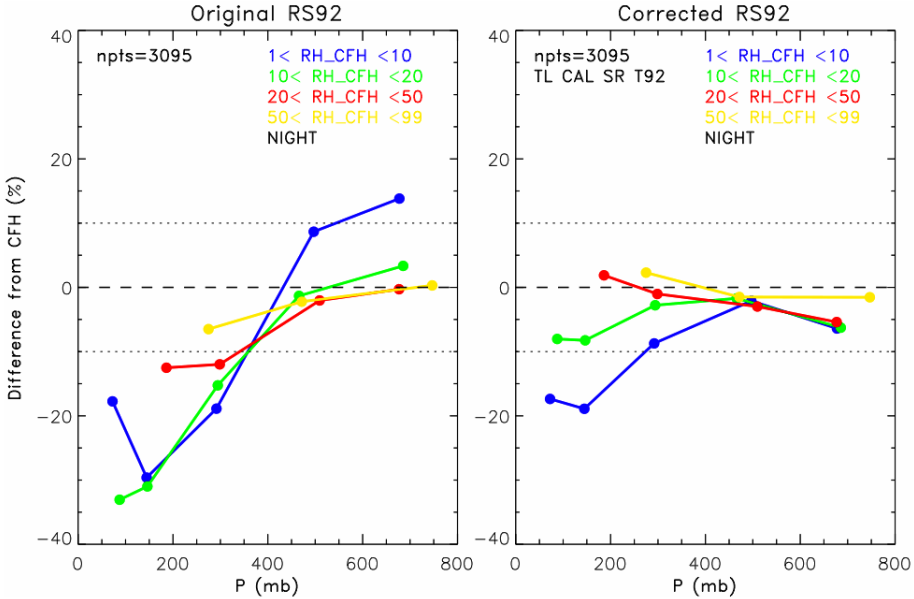

Fig. 13. RS92 mean bias relative to frostpoint hygrometer for the MOHAVE 2009 nighttime dual soundings, shown as a function of pressure (P) in 4 RH intervals, for the original RS92 measurements (left) and after applying the calibration and time-lag corrections (right).

AMTD
4, 7337–7403, 2011